National University of Science and Technology POLITEHNICA Bucharest

Faculty of Chemical Engineering and Biotechnologies

Department of Science and Engineering of Oxide Materials and Nanomaterials

PhD THESIS

Scientific coordinator:

Prof dr. ing. Anton FICAI

PhD student:
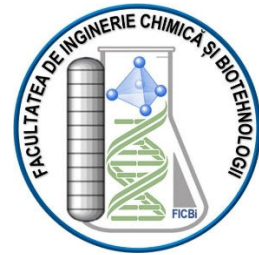
Cosmin Iulian CODREA

Bucharest

2024

National University of Science and Technology POLITEHNICA Bucharest

Faculty of Chemical Engineering and Biotechnologies

Department of Science and Engineering of Oxide Materials and Nanomaterials

FABRICATION OF 3D PRINTED SCAFFOLDS BASED ON STRONTIUM-CONTAINING

HYDROXYAPATITE COMBINED WITH POLY(E-CAPROLACTONE) AND GELATIN

METHACRYLOYL FOR BONE GRAFTING APPLICATIONS

Scientific coordinator:

Prof dr. ing. Anton FICAI

PhD student:

Cosmin Iulian CODREA

Bucharest

2024

Table of Contents

List of Abbreviations

CPC – Calcium phosphate cements

HA – Hydroxyapatite

Sr – Strontium

SrHA – Strontium-containing nano-hydroxyapatite

HT – Hydrothermal

PR – Precipitation

PLA – Poly(lactic acid)

PGA – Poly(glycolic acid)

PLGA – Poly(lactic-co-glycolic acid)

PCL – Polycaprolactone

TCP – Tricalcium phosphate

FDM – Fused Deposition Modeling

DPE – Direct pellet (granule) extrusion

DIW – Direct ink writing

SLA – Stereolithography

SLS – Selective Laser Sintering

DLP – Digital Light Processing

EBM – Electron Beam Melting

DCM – Dichloromethane

XRD – Powder X-ray diffraction

FTIR – Fourier transform infrared spectroscopy

BET – Brunauer-Emmett-Teller

TEM – Transmission electron microscopy

SAED – Selected-area electron diffraction

EELS – Electron Energy Loss Spectroscopy

SEM – Scanning electron microscopy

TGA – Thermogravimetric analysis

SBF – Simulated Body Fluid

PBS – Phosphate buffered saline

NMR – Nuclear magnetic resonance spectroscopy

CAD – Computer-assisted design

FDA – US Food and Drug Administration

BMSC – bone marrow mesenchymal stem cells

hMSC – mesenchymal stromal cells

Introduction

The mechanisms causing impaired healing are diverse and include excessive immune responses and overstrained mechanical conditions, both of which disrupt the delicate regulation needed for the early stages of healing[1]. Bone repair solutions persist as promising direction of research due to the ever-increasing demand and the limited availability of bone substitutes.

Osteoporosis is a chronic and debilitating condition marked by a decline in bone quality and mass, which makes the elderly more prone to osteoporotic fractures, also known as fragility fractures, resulting even from low-energy trauma[2]. Individuals diagnosed with osteoporosis experience a decrease in bone mineral density which elevate the risk of fractures[3] and debilitating spine deformities[4].

Current treatments primarily rely on the long-established bone grafts, including autografts, as well as allografts, and xenografts. Even so, the clinical application of these substitutes is hindered by drawbacks such as a restricted supply of donors, the need for supplementary surgical interventions, and the risks of disease propagation and immune response following implantation[5,6], as well as neurovascular damage, hematoma and seroma formation[7]. In the case of autografts, donor-site pain together with an increased operating time are unpleasant downsides[7,8].

Scaffolds from biomaterials can be used as implants but are required to conform to the characteristics of genuine bone, such as osteoinductivity, osteoconductivity, biocompatibility, and mechanical strength[5]. There are many attempts to construct new scaffolds that can replace the grafts used at this moment in clinical practice. Above we focused on materials and techniques that reproduce the desired traits and avoid several critical issues, including high expenses, the risk of growth factors to cause tumors, and the difficulty in achieving a natural integration with the adjacent normal tissue, that may cause inflammation, loosening, and osteolysis, and subsequently, implant fractures[5]. Despite encouraging clinical outcomes following the implantation of scaffolds, the issues

concerning topography, cell source and quantity, growth factor dosage and delivery method, as well as their precise mechanisms of action, remain unresolved[9].

Many Sr-based biomaterials reviewed here demonstrated enhanced new bone emergence at the implantation site and exhibited a propensity to expedite the healing when drawing a parallel to their Sr-free counterparts[10–12]. This enhancement is awaited to promote *in vivo* bone healing owing to the acknowledged anabolic and anti-catabolic attributes Sr has. The HA lattice can incorporate dissimilar ionic substitutes while maintaining the crystalline structure. HA is an essential component of genuine bone and should be included in implants designed to replicate the patient's bone for orthopedic applications[13]. Owing to their brittle and non-printability features, this sort of ceramic should be integrated with polymers to be used in the printing of bone tissue implants applications. Scaffolds with SrHA showed elevated levels of mineralization compared to both pristine PCL and PCL/HA scaffolds in *in vitro* evaluations, suggesting their potential for applications in bone tissue engineering[14]. The most favorable concentration of Sr^{2+} in composites is yet controversial[15], and choosing the adequate dose of Sr^{2+} necessary to promote bone regeneration is an issue that the present work is addressing.

Within the biomedical domain, synthetic thermoplastic polymers have gained widespread acceptance. PCL stands out as a widely utilized thermoplastic aliphatic polyester in tissue engineering due to its commendable biocompatibility and biodegradability[10]. The PCL's semicrystalline nature, attributable to its orderly structure, grants it a slow degradation rate, rendering it suitable for prolonged applications[16,17]. Moreover, the ease of processing thermoplastics enables the creation of scaffolds with adjustable mechanical properties. Optimal degradation characteristics of the scaffold and the augmentation of bioactivity are most effectively attained by integrating ceramic additives like HA, which also boost bone formation potential in vivo[18].

Hydrogels have become also promising biomaterials for tissue engineering and bone regeneration studies. Their appeal lies in their structural and compositional similarity to the extracellular matrix, elevated water content, and suitable biocompatibility. Additionally, hydrogels allow for the customization of their biophysical and biochemical

properties. Certain hydrogels also provide extra benefits such as low production costs, multifunctionality, renewability, biodegradability, and exceptional compatibility with biological systems[19].

3D-printing holds large versatility, and it can produce specific and fine implants for numerous bone augmentation applications. The design of scaffolds can be tailored to match different porosity, geometry, and surface topography in order to resemble the natural bone and to meet the demands of each specific defect[20]. Our study used a wide range of Sr concentrations in synthesized HA samples and two of the most utilized synthesis methods in order to have an extensive view on the matter and contribute to the basis of future standard practice in the field. We decided to use two popular but highly regarded 3D printing techniques with promising outcomes in the field of bone implants research, in order to contribute to their establishment as reliable solutions.

In this thesis, our goal was to design and assemble novel 3D printed composite scaffolds, with biomedical applications in treating osteoporosis affected bone, based on SrHA as carrier for the antiosteoporosis Sr ions. The first studied direction uses PCL as a structural basis and the second one uses GelMA. The motivation for the goal is based on Sr ions capability to increase osteoblast proliferation and diminish osteoclast activity. We used composite materials that combine the advantages of each component into a superior material. 3D printing was employed based on the capabilities of this group of methods to personalize implants to a degree of fine-tuning superior to all other methods.

This thesis is composed of two main parts: Part one: Critical study of the scientific literature, containing a comprehensive summary and analysis of existing research (Chapters 1 and 2), together with one review article published on the subject (Chapter 3), as well as the goals of the thesis and originality (Chapter 4), and Part two: Original contributions, containing a presentation of the methods and concepts used in the published articles presented in the thesis (Chapter 5), together with the three original research articles published (Chapter 6), and the general conclusions and perspectives (Chapter 7) and a list of publications and participations on national conferences (Chapter 8).

Part one: Critical study of the literature data

Chapter 1: Sr-containing composite materials used for 3D printed scaffolds

Polymer/HA composites are currently under investigation, including a variety of synthetic and natural polymers. Some various gelatin/HA composite products have been developed and made available for the market as porous scaffolds, fibers, and hydrogels. Recent literature reviews have indicated that combining synthetic polymers with ceramic materials can effectively mitigate each individual component limitations[21]. The main purposes of manufacturing polymer-based scaffolds containing bioactive bioceramics are making the scaffolds osteoconductive and reinforcing the scaffolds[22].

PCL is extensively used as a biomaterial due to its minimal toxicity and excellent printability while holding and FDA approval[23–25]. However, to address its inherent limitations, such as hydrophobicity, low biological interactions, and limited cell adhesion sites, several PCL-based composite biomaterials have been developed[26]. PCL has its glass transition temperature dither near -60 °C, while its melting temperature ranges between 59-64 °C[27], features that are regarded as beneficial for 3D printing[22]. PCL has a relatively constant degradation pattern due to its high-molecular weight and slow diffusion rate, a consequence of inherent hydrophobicity[28]. PCL, although biodegradable, is known to have a low degradation rate in physiological conditions[24,29], some authors mentioning two to four years in vivo in the case of larger than 1 cm^3 implants[18].

HA was successfully incorporated into 3D printed PCL/HA composite scaffolds towards 30% without significantly altering morphology or chemical composition of the scaffold. The addition of HA into PCL incrementally improved mechanical strength, cell proliferation, and mineralization[26]. The scaffolds' composition of 70% (wt.) PCL - 30% (wt.) HA was indicated to be desirable by consistently better reported results compared to scaffolds with lower HA content in terms of degradability and biocompatibility[14,24,30,31], while higher HA content is complicated to obtain via extrusion due to limitations of the method when viscosity of the material is increased[31].

Previous *in vitro* and *in vivo* studies regarding the biological activity of SrHA embedded in implants as coatings on Ti structures, membranes, gels, or tablets, have demonstrated the osteogenic effect of SrHA in relation to cell vitality, proliferation, and morphology[11,12]. Sr^{2+} is thought to promote bone regeneration by inducing macrophage polarization[15]. The findings suggest that the PCL/SrHA scaffolds can be easily build using 3D printing techniques and holds great promise as an implantable material for bone regeneration applications[16,32]. PCL/SrHA scaffolds were built by electrospinning and studies confirmed that the inclusion of SrHA microparticles increased the in vitro degradation rate of PCL[16]. Also, such composite fibers can contribute as a carrier of Sr and Ca and a sustained release of more than 28 days[33]. In vitro bioactivity studies showed enhanced dissolution rates and intense growth of apatite layer on the surface of SrHA materials when immersed in SBF and protein adsorption studies with fetal bovine serum revealed higher affinity towards SrHA materials compared to pure HA[34]. Other authors prepared a 3D printed scaffold made of PCL and SrHA to mimic the organic/inorganic components of natural bone tissue[32]. Some authors mention that biodegradation of an implanted material depends more on the passive resorption related to the dissolution rate of the composite into bodily fluids than on the active resorption due to the activity of macrophages and osteoclasts or phagocytosis[35]. The SrHA incorporation enabled the release of bioactive Sr ions and improved the compressive strength of scaffold[36]. Microporosity owed to the incorporation of a ceramic component into the composite can result in an expanded surface area in direct contact with bodily fluids, thereby hastening biodegradation and promoting apatite deposition on the material's surface, which in turn enhances the material's bioactivity[37].

The literature highlights various applications of hydrogels, including wound healing[38], vascular grafts and cardiovascular engineering[39], demonstrating their versatility in biomedical contexts. GelMA is a material synthesized from the reaction of gelatin, which is derived from collagen, and methacrylic anhydride and was also used for a variety of applications. Methacrylate or methacrylamide groups are grafted onto the hydroxyl and primary amine groups present along the gelatin backbone, facilitated by the latter. These

functional groups enable radical polymerization when exposed to UV or visible light irradiation and small amounts of a photo-initiator (such as Lithium phenyl-2,4,6-trimethylbenzoylphosphinate). This process leads to the formation of a lasting hydrogel, even at physiological temperatures, with covalent bonds within and between the polymer chains[40].

GelMA hydrogels have attained increasing attention in tissue engineering due to combining the bioactivity of gelatin with the adjustability of photo-crosslinkable hydrogels. The properties of hydrogels like stiffness, degradation rate, and bioactivity can be controlled by altering the degree of methacryloyl substitution, macromer concentration, and crosslinking conditions.

GelMA hydrogels have recently been utilized in bone and cartilage augmentation due to their excellent biocompatibility (including biosafety and biological functionality), cell adhesion, and adjustable physicochemical characteristics. The wide pores in the GelMA hydrogel network allow for the directed release of functional substances by embedding them within the GelMA matrix[41]. Additionally, incorporating bioceramics into GelMA can enhance its characteristics such as strength, cell adhesion, proliferation, osteoconductivity, and extracellular matrix deposition, which are critical for effective bone repair[42]. These composites can be engineered to exhibit tailored mechanical properties, responsiveness to temperature and magnetic stimuli, conductivity, controllable porosity, swelling, and degradability, bioactivity, expanding their potential applications[43].

A key challenge in implant development is tailoring the composite's degradation rate to align with tissue growth, up to the level of patient specific rates. Previous studies have identified several limitations with conventional synthetic hydrogels, including isotropic network structures, inadequate mechanical strength, poor adhesion to tissues, and lack of osteoconductivity. Most hydrogels act merely as carriers rather than actively promoting bone regeneration[19]. Developing multifunctional hydrogels and their composites has therefore emerged as an intriguing area of research to overcome these challenges.

Chapter 2: 3D printing

3D printing presumes constructing custom implants by precisely depositing materials layer by layer according to a predefined template[44]. It is a group of technology that offers benefits such as minimal human involvement, faster assembly, shortened design cycles, and simplified machine setup and tooling[45], as well as being cost-effective and highly reproducible[46]. This approach shows significant potential for sustainability by decreasing material waste, the stages of the product development cycle and overall the associated manufacturing costs[47].

Regarding scaffold fabrication, numerous methods are available, including both conventional (e.g., phase separation, gas foaming, solvent casting, particulate leaching) together with the more innovative 3D printing group (e.g., FDM, SLA, SLS, DLP, EBM)[48]. 3D printing enables the manufacturing of 3D constructs with precise architecture, utilizing data processed by CAD software. These methods are capable of creating complex geometries through depositing alternating layers, construction initiated from an .STL file and guided by printer software. The digital construct is split into layers or slices, gradually building a 3D construct from 2D layers that bond to each other[49]. 3D printing allows the fabrication of gradient porous structures with a multitude of designs due to the customization of pore characteristics[42]. FDM, and DLP, which are mentioned to have greatly improved the quality of biomedical products[46], are detailed bellow.

FDM is a extrusion-based technique that uses thermoplastic polymers and is the most widely used one[50]. The filaments are housed within the roller and straightforwardly linked to the extrusion head. The heating element within the extrusion head is utilized to transition the filament into a viscous liquid form prior to extruding it through the nozzle onto the printing zone to create the final element. The incoming solid filament functions as a plunger, pushing and extruding the molten feedstock through the nozzle[51,52]. An important note is that FDM is mostly the same method as FFF and can be used interchangeably[53,54]. Other extruder designs, such as ram, screw or syringe-style printers, also fall within the FDM family[52]. A variation of the FDM is DPE which uses DPE pellets of materials for

extrusion. DPE is a material extrusion technique using thermoplastic polymers that is simpler and more economical. DPE printing eliminates certain intermediate stages, making the process cheaper and more versatile[55]. This class of extrusion operates by melting the material found inside a small keg and using a plunger to force it out at a controlled rate[52]. Other authors mention the same technique as DIW or bioplotting. DIW or pressure-driven printing, employs a pneumatic or mechanical (with the help of a piston or screw) dispensing system to extrude molten materials, solutions, gels, or suspensions through a nozzle or syringe. DIW is cited to be the most prevalent technique for bioprinting cell suspensions, cell-laden hydrogels, and extracellular matrix-based solutions[56].

DLP printing entails the step-by-step crosslinking of photosensitive inks under projection patterns. DLP involves the photochemical linking of small monomers in a chain-like fashion to create a solid object[48]. DLP offers advantages such as increased speed, straightforward manipulation of mechanical properties, and scalable resolution down to 1 µm, surpassing other techniques[57]. DLP addresses the existing obstacles in rapidly fabricating tissue building blocks with high precision, enabling the production of scaffolds at clinically significant pace. The printing speed of DLP surpasses that of extrusion 3D printing[57]. With DLP printing, a digital light projector rapidly renders intricate layer images of the desired 3D shape. Light-based DLP and SLA are already embraced in the field of dentistry, where 3D scanners and 3D printers are employed to create patient-specific crowns, surgical implants, mouthguards, and retainers[58].

While 3D printing techniques have become powerful tools for scaffold fabrication, reproducibility and quality control are crucial challenges that must be addressed to transition 3D printed scaffolds to clinical use[31]. Alongside material selection, factors such as scaffold components, composition refinement, architectural properties, and biomimetic design play significant roles in governing the bioactivity that aids in bone remodeling and regeneration[10]. 3D constructs produced by different techniques, while using of same composite material, exhibited notable differences in morphology, surface roughness, internal void fraction, and degradation rates. These variations led to distinct mechanical properties and cell responses[28].

Review

Advances in Osteoporotic Bone Tissue Engineering

Cosmin Iulian Codrea [1,2], Alexa-Maria Croitoru [1], Cosmin Constantin Baciu [3], Alina Melinescu [1,*], Denisa Ficai [4], Victor Fruth [2] and Anton Ficai [1,5]

[1] Department of Science and Engineering of Oxide Materials and Nanomaterials, Faculty of Applied Chemistry and Materials Science, University POLITEHNICA of Bucharest, 060042 Bucharest, Romania; codrea.cosmin@yahoo.com (C.I.C.); croitoru.alexa@yahoo.com (A.-M.C.); anton.ficai@upb.ro (A.F.)

[2] Department of Oxide Compounds and Materials Science, Institute of Physical Chemistry "Ilie Murgulescu" of the Romanian Academy, 060021 Bucharest, Romania; vfruth@gmail.com

[3] Anaesthesia Intensive Care Unit (AICU/ATI), Department of Orthopedics, University of Medicine and Pharmacy "Carol Davila", 020021 Bucharest, Romania; cosminbaciu@hotmail.com

[4] Department of Inorganic Chemistry, Physical Chemistry and Electrochemistry, Faculty of Applied Chemistry and Materials Science, University POLITEHNICA of Bucharest, 060042 Bucharest, Romania; denisaficai@yahoo.ro

[5] Academy of Romanian Scientists, 050094 Bucharest, Romania

* Correspondence: alina.melinescu@gmail.com

Abstract: The increase in osteoporotic fracture worldwide is urging bone tissue engineering research to find new, improved solutions both for the biomaterials used in designing bone scaffolds and the anti-osteoporotic agents capable of promoting bone regeneration. This review aims to report on the latest advances in biomaterials by discussing the types of biomaterials and their properties, with a special emphasis on polymer-ceramic composites. The use of hydroxyapatite in combination with natural/synthetic polymers can take advantage of each of their components properties and has a great potential in bone tissue engineering, in general. A comparison between the benefits and potential limitations of different scaffold fabrication methods lead to a raised awareness of the challenges research face in dealing with osteoporotic fracture. Advances in 3D printing techniques are providing the ways to manufacture improved, complex, and specialized 3D scaffolds, capable of delivering therapeutic factors directly at the osteoporotic skeletal defect site with predefined rate which is essential in order to optimize the osteointegration/healing rate. Among these factors, strontium has the potential to increase osseointegration, osteogenesis, and healing rate. Strontium ranelate as well as other biological active agents are known to be effective in treating osteoporosis due to both anti-resorptive and anabolic properties but has adverse effects that can be reduced/avoided by local release from biomaterials. In this manner, incorporation of these agents in polymer-ceramic composites bone scaffolds can have significant clinical applications for the recovery of fractured osteoporotic bones limiting or removing the risks associated with systemic administration.

Keywords: bone; biomaterial scaffolds; 3D printing; osteoporosis; strontium ranelate

1. Introduction

Bone grafting is a common surgical method used to improve bone regeneration in orthopedic practice. In the case of considerable diminution of bone mass, bone grafts are essential because the self-healing process would be slow or the could entirely fail [1]. At an estimated total of 2,000,000 bone graft procedures carried out every year, bone repair frameworks remain a promising line of research because of the continuously growing request for it and the reduced stock of bone substitutes [1,2]. Bone tissue engineering aims at delivering novel methods for treating bone tissue deficiencies often resulting from polytrauma, pathological fractures, and osteonecrosis [2] as there is an increasing need to provide functional replacement grafts for the patients [3].

Chapter 4. Goals of the thesis and originality

This thesis aims to develop multi-layered 3D printed scaffolds comprised of 70% wt. PCL and 30% wt. SrHA through FDM technique, as well as 10% w/v GelMA and 5% w/v SrHA through DLP technique, both with different Sr concentrations. Two kinds of HA/SrHA, dissimilar in shape (rod-like and spherical), were synthesized via distinct methods, PR and HT, and thoroughly characterized chemically and morphologically. Also, for each type of SrHA, we employed a large interval of Sr content, namely the Sr/(Ca + Sr) molar ratios of 1, 5, 10, 20, and 30%.

The novelty of this thesis consists of the development of innovative 3D printed scaffolds from SrHA composite materials, for controlled long-term release of Sr in the desired bone situs, while supplementary comparing the effect PR and HT synthesis methods and different Sr content have on the composite scaffold properties. The new 3D printed scaffolds with improved physico-chemical and biological properties are designed for repairing bone defects, especially those caused by osteoporosis, and to lower the side effects in comparison with the oral administration of Sr ranelate as an antiosteoporosis medicine.

Therefore, in the current thesis, two research directions are considered, based on the anti-osteoporotic properties of SrHA:

1. Developing of effective and novel FDM 3D printed 70% wt. PCL and 30% wt. SrHA composite scaffolds, SrHA was incorporated into the PCL lattice to augment the surface characteristics and bioactivity of the scaffolds. The additional filament surface morphology increased the exposure and availability of the ceramic particles, leading to a beneficial synergistic effect on surface properties. This resulted in a notable enhancement in bio-mineralization. While similar studies involving PCL and HA are quite abundant, the combination of PCL and SrHA is less studied and, to the best of our knowledge the exact content and design of this type of scaffolds was not used before to compare the effect of two different kinds of SrHA synthesis.

2. Developing of effective and novel DLP 3D printed 10% (w/v) GelMA and 5% (w/v) SrHA composite scaffolds. SrHA was incorporated into the GelMA matrix to augment the mechanical characteristics and swelling and degradation performance of the scaffolds. Although studies regarding DLP 3D printed GelMA and HA composite scaffolds, the research on GelMA and SrHA is scarce, and the exact combination of content and design is unique. The comparison between the effects of the two different kinds of SrHA synthesis have on scaffold properties adds up to the novelty of the thesis.

The main objectives were accomplished through several intermediate objectives, as detailed beneath:

- Synthesis of HA/SrHA nanomaterials, with the intent of using HA as control while using SrHA as a source of Sr for bone regeneration;

- Morphological, structural and biological characterization of HA/SrHA nanomaterials;

- Development of composite PCL and SrHA scaffolds though CAD design and multiple 3D printing iterations;

- Morphological, structural and biological characterization of composite PCL and SrHA scaffolds;

- Development of composite GelMA and SrHA scaffolds though CAD design and multiple 3D printing iterations;

- Morphological, structural and biological characterization of composite GelMA and SrHA scaffolds.

All the results obtained in our research activities described below were published in peer-reviewed journals. In regard to the completion of this thesis, four articles were published, with the PhD student as first author (one was a review paper and three of them were original research articles). The review paper details the motifs in choosing SrHA as a anti osteoporotic agent, while the original articles present the designing of novel 3D printed composite scaffolds based on SrHA, with different Sr concentrations, synthesized through co-PR and HT methods.

Part two: Original contributions

Chapter 5: Materials and Methods

Materials

For the synthesis of HA and SrHA, $Ca(NO_3)_2 \cdot 4H_2O$, Sigma Aldrich, $Sr(NO_3)_2$, Fluka, and $(NH_4)_2HPO_4$, Sigma Aldrich, were used as precursors. Poly(ε-caprolactone) pellets (average mol wt 45 kDa) were purchased from Sigma Aldrich. For GelMA synthesis we used as reagents gelatin (type A) sourced from porcine skin, Sigma Aldrich (average mol wt 50—100 kDa) and methacrylic anhydride, Sigma Aldrich (mol wt 154.16 g/mol). Lithium phenyl-2,4,6-trimethylbenzoylphosphinate (mol wt 294.10 g/mol) served as the photoinitiator. All used substances were graded for analytical purposes and further details are available in the published articles included in the thesis below in Chapter 6.

Characterization methods

In this section the characterization methods used in our research were described. We focused on the general principles in order to gain a thorough comprehension of the motifs behind their usage in investigating both HA/SrHA powders and composite scaffold's properties. Further details about their explicit usage in our research are available in the published articles included in the thesis below in Chapter 6.

Scaffold design and printing

For the first studied direction (PCL/SrHA), our research group worked on the 3D Bioplotter®, which is considered the earliest commercial 3D bioprinter. The 3D Bioplotter® can print cell-laden hydrogels such as gelatin, fibrin, alginate, and agarose, as well as polymers and inorganic ceramic materials like PCL, HA, and TCP particles to create scaffolds[59].

CAD files are essential in 3D printing, forming the foundation of the process. CAD software is used to generate STL files, which serve as input for the printer software. In our work also, the initial step involved designing cylindrical structures with a diameter of 10

mm and a height of 2.52 mm with the help of Bioplotter RP 3.0 software. The structures were then sliced with the appropriate layer thickness, typically lower than the needle tip diameter. A layer thickness of 360 μm was selected, slightly smaller than the needle tip inner diameter of 400 μm.

The 3D object was constructed using the BPL files, which are used to save the sliced project and are compatible with the Visual Machines software. After assigning material to the robot head, the device proceeded printing the cylindrical scaffold. The PCL-based composites were made using 70% w/w PCL (Mn 45000) and 30% w/w HA/SrHA. To ensure better dispersion of HA, a 45 μm sieve was used before mixing it with PCL. Composite materials were placed into the stainless-steel syringe of the dispense head and heated to 130°C for 15 minutes to achieve a homogeneous molten state. Cylindrical scaffolds were printed at a constant temperature layer by layer to create a circular grid structure. The distance between strands was adjusted to 0.6 mm. Strand diameter was adjusted to 0.4 mm (needle inner diameter). The gap separating the strands point to the pore size of every scaffold and was set to 0.4 mm.

For the second studied direction (PCL/SrHA), our research group has been working on Anycubic Photon D2 which uses the DLP, with mirrors that concentrate the light directly to the bottom of the resin vat. Although this 3D printer is rated as being a consumer-grade one[60], it was used on other studies of bone regeneration applications[61]. It has a user-friendly touchscreen interface which simplifies operation, making it very accessible.

The printer's software converts 3D models into sliced layers, guiding the light projection for each layer. Computer-aided design (CAD) files containing the instructions for the scaffolds were designed employing SolidWorks, saved as .stl files and sliced via Chitubox, the embedded software of the DLP-based Anycubic's Photon D2 3D Printer. Scaffolds were designed to be 18 × 18 × 1.3 mm in size and containing 3 x 3 macropores, for the purpose of showing the printability capacities of the material (Figure 7). The distance between pores was set to 3 mm. Pore side size was set to 2 mm. Side size was set to 18 mm. Samples were lyophilized before further analyses. SEM images indicate that the samples kept a similar shape with the one intended through 3D printing (Figure 8).

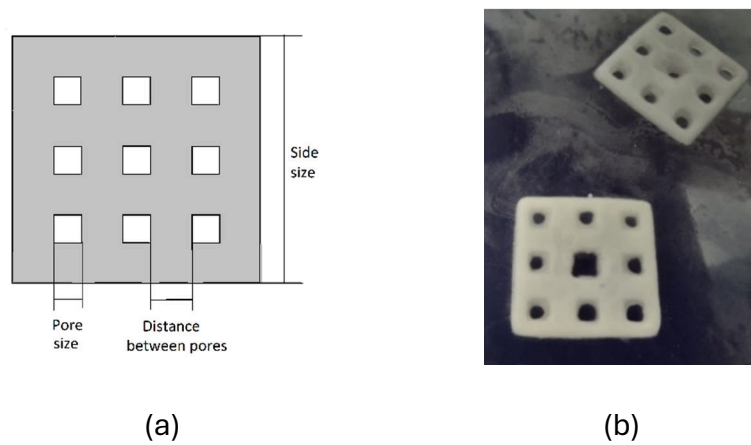(a)   (b)

Figure 7. Schematic illustration of scaffolds (a) and representative macroscopic image (b).

The foremost difficulty in scaffold-driven bone regeneration is to secure adequate blood supply to circumvent potential deficiencies in neovascularization, subsequent ischemia, and necrosis. Approaches to address these difficulties include accelerating angiogenesis within the scaffold or utilizing existing vascularization to ensure sufficient blood supply. Scaffold design characteristics like porosity, pore size and interconnectivity are vital for enabling the infiltration of pre-existing vessels and vessel-forming cells.
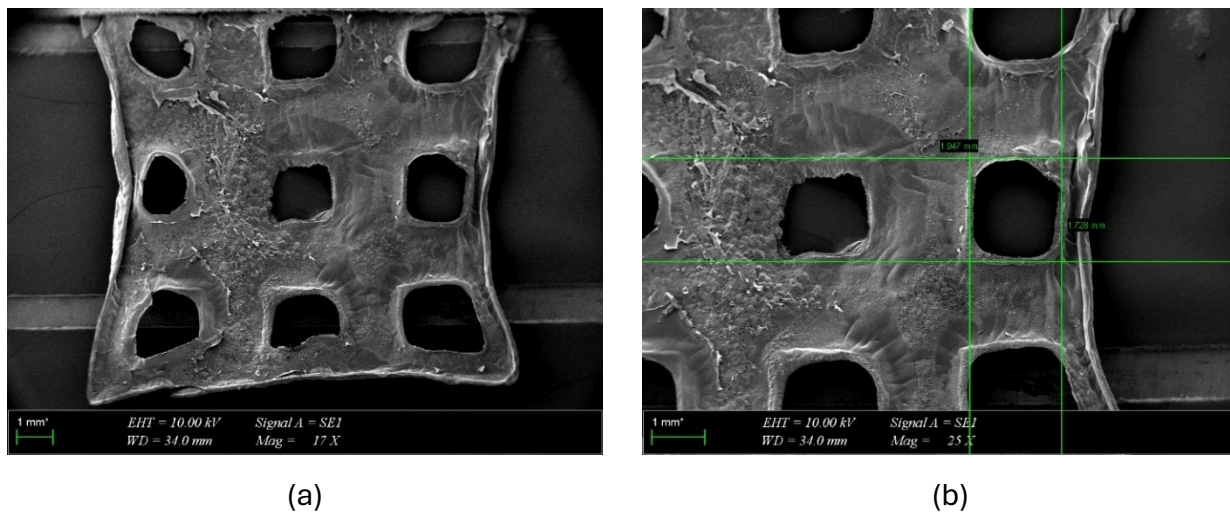

(a)   (b)

Figure 8. GelMA scaffolds after lyophilization. Representative SEM images at: (a) magnification 17 X, (b) magnification 25 X.

Article

Three-Dimensional-Printed Composite Scaffolds Containing Poly-ε-Caprolactone and Strontium-Doped Hydroxyapatite for Osteoporotic Bone Restoration

Cosmin Iulian Codrea [1,2], Daniel Lincu [1,2], Vladimir Lucian Ene [1,3,4,*], Adrian Ionuț Nicoară [1,3,4], Miruna Silvia Stan [5], Denisa Ficai [1,3,4] and Anton Ficai [1,3,4,6]

1   Faculty of Chemical Engineering and Biotechnologies, National University of Science and Technology Politehnica of Bucharest, 060042 Bucharest, Romania; ccodrea@icf.ro (C.I.C.); daniel.lincu1113a@gmail.com (D.L.); adi.nicoara18@gmail.com (A.I.N.); denisaficai@yahoo.ro (D.F.); anton_ficai81@yahoo.com (A.F.)
2   Institute of Physical Chemistry "Ilie Murgulescu" of the Romanian Academy, 060021 Bucharest, Romania
3   National Research Center for Micro and Nanomaterials, Faculty of Chemical Engineering and Biotechnologies, National University of Science and Technology Politehnica of Bucharest, Splaiul Independentei 313, 060042 Bucharest, Romania
4   National Centre for Food Safety, National University of Science and Technology Politehnica Bucharest, Splaiul Independentei 313, 060042 Bucharest, Romania
5   Department of Biochemistry and Molecular Biology, Faculty of Biology, University of Bucharest, Splaiul Independentei 91-95, 050095 Bucharest, Romania; miruna.stan@bio.unibuc.ro
6   The Academy of Romanian Scientists, Ilfov St. 3, 050044 Bucharest, Romania
*   Correspondence: vladimir.ene@upb.com

Abstract: A challenge in tissue engineering and the pharmaceutical sector is the development of controlled local release of drugs that raise issues when systemic administration is applied. Strontium is an example of an effective anti-osteoporotic agent, used in treating osteoporosis due to both anti-resorptive and anabolic mechanisms of action. Designing bone scaffolds with a higher capability of promoting bone regeneration is a topical research subject. In this study, we developed composite multi-layer three-dimensional (3D) scaffolds for bone tissue engineering based on nano-hydroxyapatite (HA), Sr-containing nano-hydroxyapatite (SrHA), and poly-ε-caprolactone (PCL) through the material extrusion fabrication technique. Previously obtained HA and SrHA with various Sr content were used for the composite material. The chemical, morphological, and biocompatibility properties of the 3D-printed scaffolds obtained using HA/SrHA and PCL were investigated. The 3D composite scaffolds showed good cytocompatibility and osteogenic potential, which is specifically recommended in applications when faster mineralization is needed, such as osteoporosis treatment.

Keywords: hydroxyapatite nano-powder; co-precipitation; hydrothermal; strontium; poly-ε-caprolactone; 3D printing; bioactivity

1. Introduction

An increasing number of researchers have turned their attention to making new materials with controllable properties and interactions for bone tissue regeneration. These biomaterials should mimic not only the bone composition and its micro and nanostructure, but also its functions, while taking into account the different needs of each patient [1]. Osteoporotic patients are particularly prone to challenging complications as it is known that healing time and failure rate are increased for them. They require supplementary pharmacological measures to improve bone healing in the short term and overall quality in the long term [2]. Hydroxyapatite (HA) is extensively used as a bone graft material in both orthopedic and dental applications due to its capacity to form strong bonds to natural bone tissue [3]. Its main disadvantages are inherent brittleness [4], low mechanical properties

2.3.2. Thermogravimetric (TG) Analysis

TG was performed using a Mettler Toledo TGA/SDTA851e instrument under 80 mL/min synthetic air flow, using open ceramic pans. The heating rate was adjusted at 10 °C/min and the temperature range was between 25° C and 800° C.

2.3.3. Scanning Electron Microscopy (SEM) Analysis

SEM measurements were performed using a field emission gun scanning electron microscope (FEG-SEM) Quanta Inspect F50, with a resolution of 1.2 nm. The surface morphologies of the scaffolds as well as the size of the fibers were observed. Sample preparation included liquid nitrogen immersion and breaking of scaffolds using gentle pestle hits, gold coating, and subsequently fixation of sample on aluminum stubs by using carbon tape. The images were collected through the equipment's software. To determine the average strand and pore diameters (Feret's diameter) from SEM images, ImageJ 1.54d software (National Institutes of Health, Bethesda, MD, USA) was used.

2.3.4. Mechanical Properties

All tests were performed on cylindrical samples at room temperature using the Shimadzu Autograph AGS-X 20kN (Shimadzu, Tokyo, Japan) testing machine. The diameter and thickness of all samples were measured before testing. Testing was conducted at a constant loading rate of 0.5 mm/min and a maximum loading of 4000 N.

2.3.5. In Vitro Chemical Bioactivity

Bioactivity was evaluated after immersing the scaffolds in simulated body fluid (SBF) solution at 37 °C for 28 days with the help of SEM coupled with EDX spectroscopy, as well as through measuring throughout the experiment the weight of the scaffolds, the pH, and conductivity of the SBF. An inoLab Multi 9630 IDS (Xylem, Washingtonc, DC, USA) pH meter was used. The preparation of the SBF solution was performed according to Kokubo's recipe and procedure [29]. The SBF was not refreshed during the experiment. After immersion, the scaffolds were removed from the SBF medium, rinsed with deionized water, and dried at room temperature. The samples were analyzed using SEM and energy-dispersive X-ray (EDX) to determine the formation of the apatite layer on the surface of the scaffolds after 28 days.

2.3.6. In Vitro Biological Evaluation

Mouse pre-osteoblasts (MC3T3-E1 cell line) were grown in Dulbecco Modified Eagle's Medium (Invitrogen, Waltham, MA, USA) with 10% fetal bovine serum (Gibco, Waltham, MA, USA) at 37 °C in a humidified atmosphere with 5% CO_2. The cells were seeded at a cell density of 6×10^4 cells/cm^2 on the tissue culture plastic surface (TCPS) which served as a control, on the top of the PCL 70% (wt.)–HA/SrHA 30% (wt.) scaffolds which were previously sterilized under UV light for 2 h. After 24 h of incubation in standard conditions, the biocompatibility tests were performed.

The cellular viability was measured using the 3-(4,5-dimethylthiazol-2-yl)-2,5-diphenyltetrazolium bromide (Sigma-Aldrich, St. Louis, MO, USA) assay (MTT). The culture medium was removed at the end of incubation time and the cells were incubated with 1 mg/mL MTT solution for 2 h at 37 °C. The purple formazan crystals formed in the viable cells were dissolved with 2-propanol (Sigma-Aldrich, St. Louis, MO, USA) and the absorbance was measured at 595 nm using a microplate reader (FlexStation 3, Molecular Devices, Sunnyvale, CA, USA).

The concentration of nitric oxide (NO) in the culture medium collected after the 24 h of incubation was measured using the Griess reagent, a stoichiometric solution (v/v) of 0.1% naphthylethylendiamine dihydrochloride, 1% sulfanilamide in 5% phosphoric acid. The absorbance of the mix formed by equal volumes of medium supernatants and Griess reagent was read at 550 nm using a microplate reader and the NO concentration was calculated from the $NaNO_2$ standard curve.

21

The culture medium was harvested after 24 h of osteoblasts' growth in the presence of tested samples and used for lactate dehydrogenase (LDH) release measurement with Cytotoxicity Detection KitPLUS (Roche, Indianapolis, IN, USA), following the manufacturer's instructions. Volumes of 100 μL culture supernatants were mixed with 100 μL mix of catalyst and dye solution and incubated for 20 min in a dark place. After the reaction was stopped, the absorbance was read at 490 nm using a microplate reader (Flex Station 3, Molecular Devices, Sunnyvale, CA, USA).

Following incubation, the cells were fixed with 4% paraformaldehyde for 20 min and permeabilized with 0.1% Triton X-100 2% bovine serum albumin for 45 min. The actin filaments were stained with 10 μg/mL phalloidin-FITC (fluorescein isothiocyanate) and the nuclei were counterstained with 2 μg/mL DAPI (4',6-diamino-2-phenylindole). An Olympus IX71 inverted fluorescence microscope was used to capture the images.

The in vitro assays were performed in triplicates and the results were calculated as mean ± standard deviation (SD) of three independent experiments. The statistical analysis was carried out on three replicates per sample by the unpaired Student t-test, and differences were considered significant for a *p*-value less than 0.05.

2.3.7. Statistical Analysis

Data are represented as mean ± standard deviation (S.D.). The graphs and statistical analysis were performed using MS Excel software for Microsoft 365 (Version 2404). Data were compared using one-way analysis of variance (ANOVA), followed by a two tails *t*-test. Values of $p < 0.05$ were considered statistically significant.

3. Results and Discussion

3.1. PCL 70% (wt.)–HA/SrHA 30% (wt.) Scaffolds Design

The macro-morphology of PCL, PCL-HA, and PCL–SrHA scaffolds (Figure 1a,b) indicate good compliance with the CAD model. The scaffolds exhibit a regular macroscopic porous structure and are stacked layer by layer. The strands are well defined and clearly observed both macroscopically and microscopically (Figure 1c). There was no obvious difference between the scaffolds.
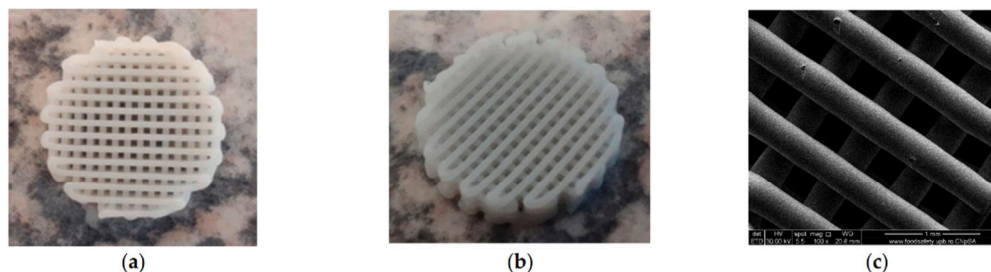

(a)   (b)   (c)

Figure 1. PCL 70% (wt.)–SrHA 30% (wt.) scaffolds obtained using HAHTSr10% powder: (**a**) macroscopic top-view, (**b**) macroscopic lateral-view, (**c**) top-view SEM images in EDT mode.

A higher specific surface area has a direct relationship with the increase in the adsorption of macromolecules and proteins, particularly involved with the induction of osteogenesis. The diameter of interconnected pores is recommended to be at least 300 μm to allow proper cell migration inside the grafts and proper angiogenesis, which are two of the most important aspects for new-bone formation inside existing pores [30]. Macropores of the obtained scaffolds were measured from the SEM micrographs using ImageJ 1.54d software (Figure 2) and the obtained results follow the recommendations found in the literature, with mean diameter of pores varying between 230–320 μm. The results are similar, with statistically significant differences only for the samples with 1%Sr.
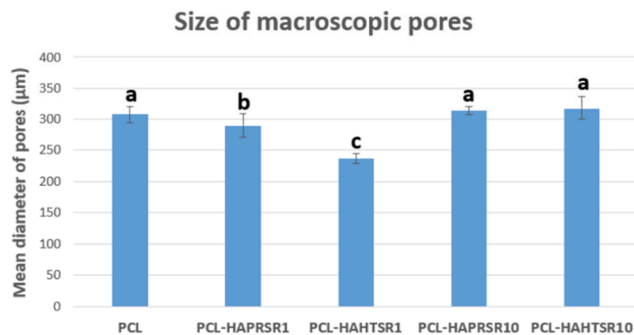
Figure 2. Macropore diameter measurements on PCL and 70% PCL–30% SrHA composites. Results are represented as mean ± SD; different letters indicate significant differences between each sample ($p < 0.05$).

3.2. Thermogravimetric (TG) Analysis

TG measurements were conducted on the 3D-printed scaffolds to quantify the HA/SrHA content at the end of the scaffold fabrication process. A sample of ~12 mg in weight was heated to 800 °C at a rate of 10 °C/min, and the sample weight loss was recorded over time. In addition, for control, a PCL pellet (~15 mg in weight) was tested in the same way. TG analysis was used to assess the composition (wt%) of the composite materials prepared through the melt-blending technique, as well as their thermal stability. All composite materials had experimental compositions close to the design value of 70% wt. PCL and 30% wt. HA/SrHA, as seen in Table 1. All the scaffolds demonstrated a one-step decomposition profile with a single transition temperature and similar thermal stability, with decomposition starting around 250 °C; however, the scaffolds printed with HA/SrHA material appeared to finish degradation at a lower temperature compared to the simple PCL scaffolds, as seen in Figure 3, for composites containing HAPRSr10% and HASR10%. This may be due to a catalytic effect of these powders and most likely a better thermal conductivity within the mass.

Table 1. TG measurements on 70% PCL–30% HA/SrHA composites.

| Sample Name	Powder Synthesis Method	Powder Sr/(Ca+Sr) Molar Ratio (%)	Determined Content in the Scaffold (% wt.)	
			HA/SrHA	PCL
PCL-HAPRSr1	Precipitation	1	28.7	71.3
PCL-HAPRSr5		5	29.2	70.8
PCL-HAPRSr10		10	28.7	71.3
PCL-HAPRSr20		20	28.4	71.6
PCL-HAPRSr30		30	27.3	72.7
PCL-HAHTSr1	Hydrothermal	1	29.1	70.9
PCL-HAHTSr5		5	28.8	71.2
PCL-HAHTSr10		10	29.4	70.6
PCL-HAHTSr20		20	28.7	71.3
PCL-HAHTSr30		30	28.8	71.2
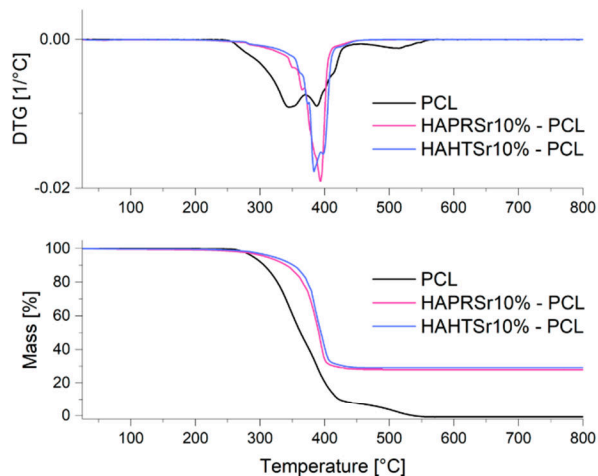
Figure 3. TG/DTG measurements on PCL and composite scaffolds containing HAPRSr10% and HAHTSr10%.

Considering the fact that ceramic component HA/SrHA is the only component that does not decompose during the TGA process, it can be assumed that during the entire processing, no heterogeneities are obtained, and the final composition is close to the desired one, for all the samples obtained with precipitated or hydrothermal HA/SrHA.

3.3. Scanning Electron Microscopy

To investigate the obtained scaffolds' surface morphology and strands' dimensions, SEM analysis was performed. Morphological evaluation of the 3D-printed scaffolds at different magnifications showing strands and surfaces indicate that the printed scaffolds displayed a high level of fidelity to the original CAD model (Figures 4–6), with completely open and interconnected pore architecture. Strand diameter was measured using ImageJ 1.54d software for several samples (Figure 7) and the average value was close to the theoretical target value of the printing needle (400 μm). Simple PCL strands had statistically significant bigger values than the composite strands due to the typical behavior of viscoelastic polymer-based biomaterial inks, that tend to expand upon extrusion from the nozzle [31]. However, no significant differences were observed between the composites containing 10%Sr.
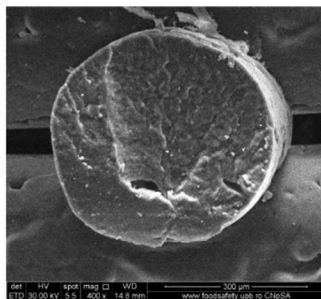

Figure 4. Cross-section SEM images of 100% PCL scaffolds.

24

Images acquired at higher magnification using a top-view scan and the backscattered electron (CBS) mode evidenced the presence of SrHA particles and micro-porosity on the surface of all analyzed samples (Figure 8). Composite filaments' surface appeared less smooth than the simple PCL. More and smaller micropores can be observed in the case of composite scaffolds, compared with simple PCL scaffolds. This might be due to the collision of ceramic particles with PCL crystalline regions growing during solidification, as other authors mention [32]. Cross-section images, even on lower magnification, indicate the agglomeration or clumping of the ceramic particles in the composite-based samples in both CBS and Everhart–Thornley Detector (ETD) modes (Figures 5 and 6) but there is no critical agglomeration which means that homogenous materials were obtained.
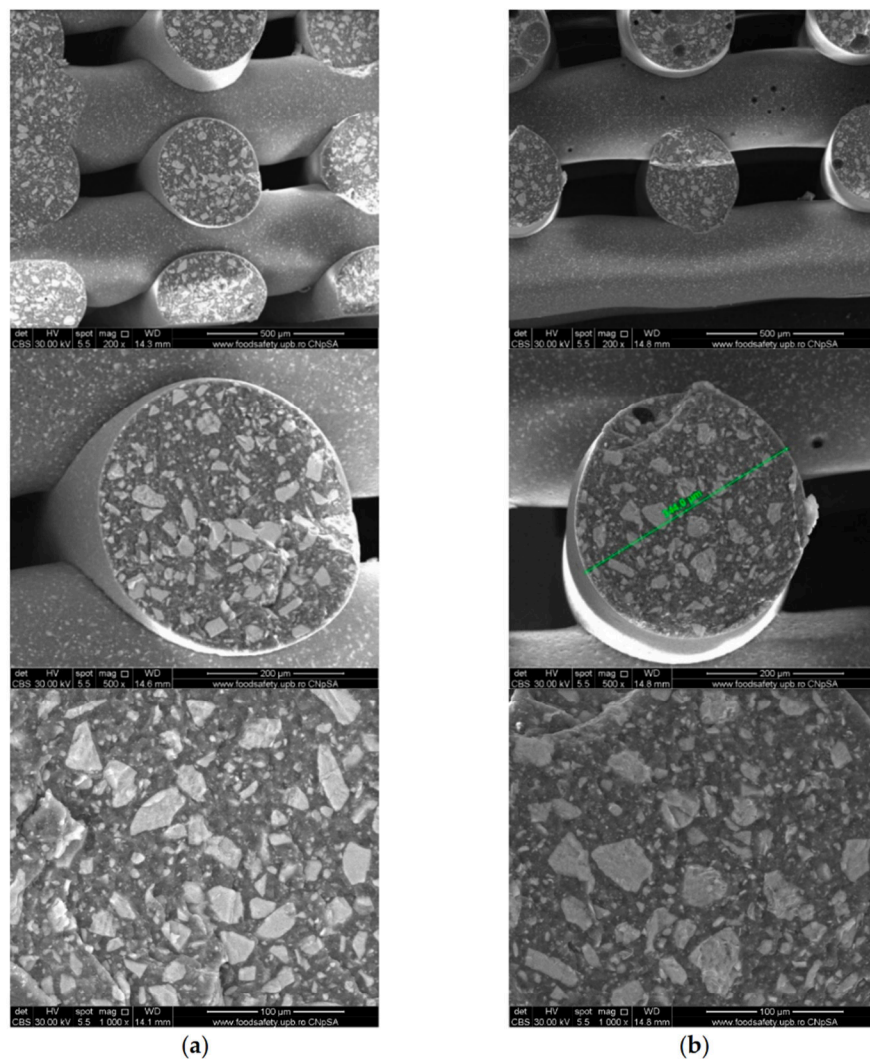

(**a**) (**b**)

Figure 5. Cross-section SEM images of 70% PCL–30% SrHA composite scaffolds (**a**) PCL–HAPR-Sr1%, (**b**) PCL–HAPR-Sr10%.
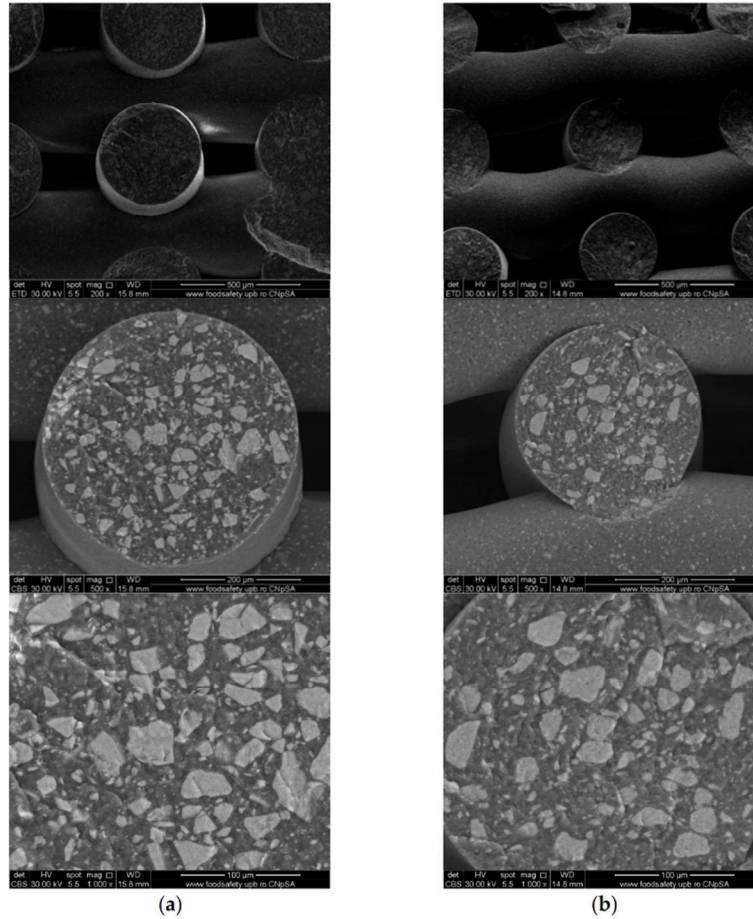
Figure 6. SEM images of 70% PCL–30% SrHA composite scaffolds (**a**) PCL–HAHT-Sr1%, (**b**) PCL–HAHT-Sr10%.
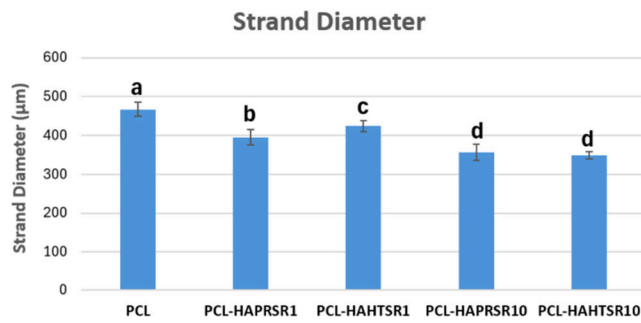

Figure 7. Strand diameter measurements on PCL and 70% PCL–30% SrHA composites. Results are represented as mean ± SD; different letters indicate significant differences between each sample ($p < 0.005$).
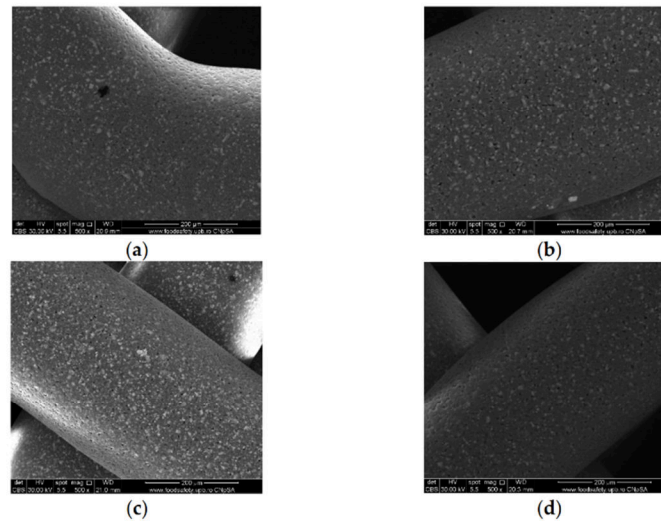
Figure 8. Top-view SEM images of 70% PCL–30% SrHA composite scaffolds (**a**) PCL–HAPR-Sr1%, (**b**) PCL–HAHT-Sr1%, (**c**) PCL–HAPR-Sr10%, (**d**) PCL–HAHT-Sr10%.

The surface of the samples (top-view) is very important because this is in direct contact with the surrounding fluids, cells, and tissues. The surfaces reveal HA particles partially embedded into the polymer matrix but also micrometric pores. The surface roughness is important because it can allow a better cell–graft interaction and thus a better cell attachment onto the surface. Pores were analyzed quantitatively by ImageJ and presented using average Feret diameter (Figure 9). The average size was similar in all composite samples, with no statistically significant differences, but statistically different from the PCL sample that presented pore shape polydispersity and a higher average diameter. These measurements indicate that the observed pores are in the optimal diameter range for cell adhesion (1–10 μm in diameter), similar to the microstructure of tissue- and organ-derived decellularized extracellular matrices [33]. Surface pores of 3–12 μm size are important for direct cell–cell contacts, migration, and/or invasion [34]. Together with the larger macropores intentionally obtained via CAD design, these smaller pores create a multiscale pore architecture that substantially promotes cell adhesion, viability, and proliferation.
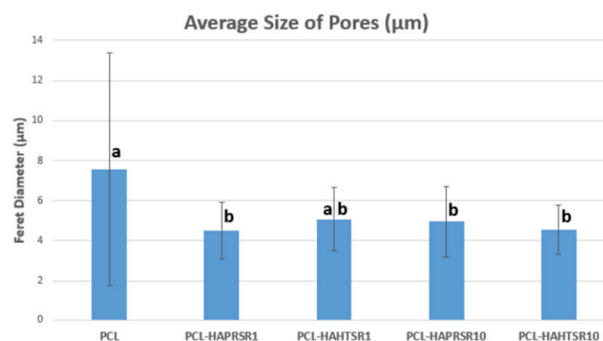

Figure 9. The average size of pores using Feret diameter measurements on PCL and 70% PCL–30% SrHA composite samples. Results are represented as mean ± SD; different letters indicate significant differences between each sample ($p < 0.05$).

depicted in Figures 15 and 16. Prior to immersion, surface features like pores and roughness remained unchanged by the SBF. However, a continuous apatite coating, approximately 6 μm thick, was detected on all scaffolds, supported by EDS spectra and mapping (Figure S1, Supporting Information). Notably, a tendency for cracking or exfoliation of the apatite layer was observed across all samples, indicating potential inadequate adhesion between the scaffold surface (particularly PCL) and the mineral coating. Factors such as pH variations, ion exchange, and scaffold component dissolution (HA) may influence the stability and integrity of the mineral coating. Cross-section SEM images revealed apatite-filled pores within the scaffold and the formation of micronic agglomerates. These results imply the scaffolds' effectiveness in promoting mineralization, yet underscore the need for further optimization of fabrication protocols and material design strategies to improve adhesion and durability of the apatite layer on 3D-printed scaffolds.
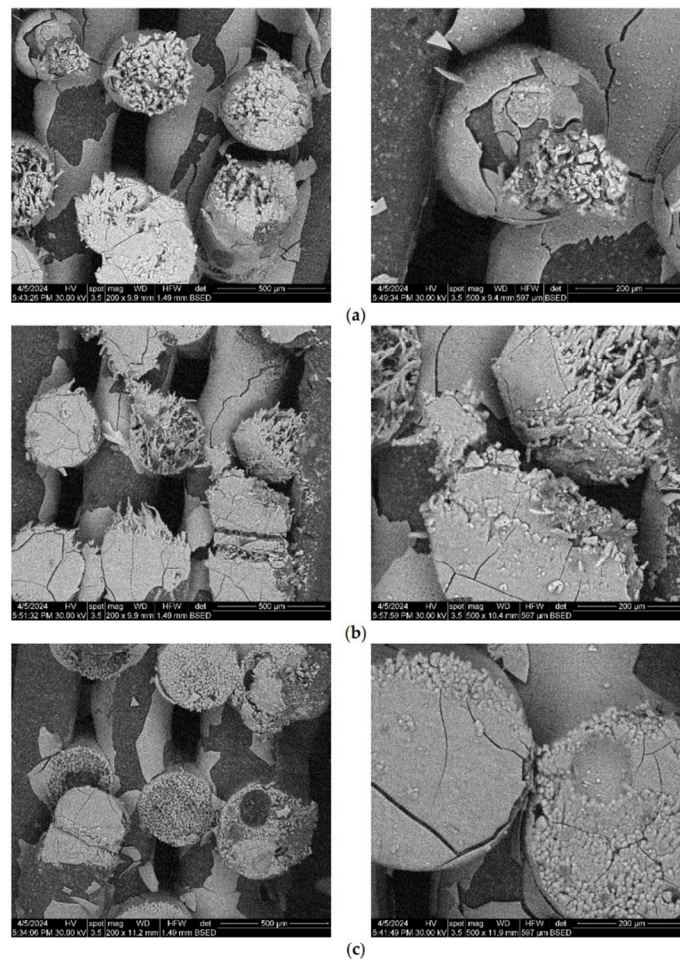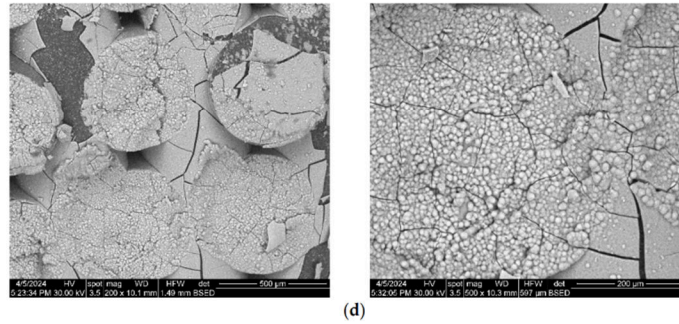

Figure 15. *Cont.*

(**d**)

Figure 15. SEM images of the 3D-printed composite scaffolds containing precipitation-obtained SrHA after 28 days of immersion in SBF: (**a**) PCL-HAPR-Sr1%, (**b**) PCL-HAPR-Sr5%, (**c**) PCL-HAPR-Sr10%, (**d**) PCL-HAPR-Sr20%.
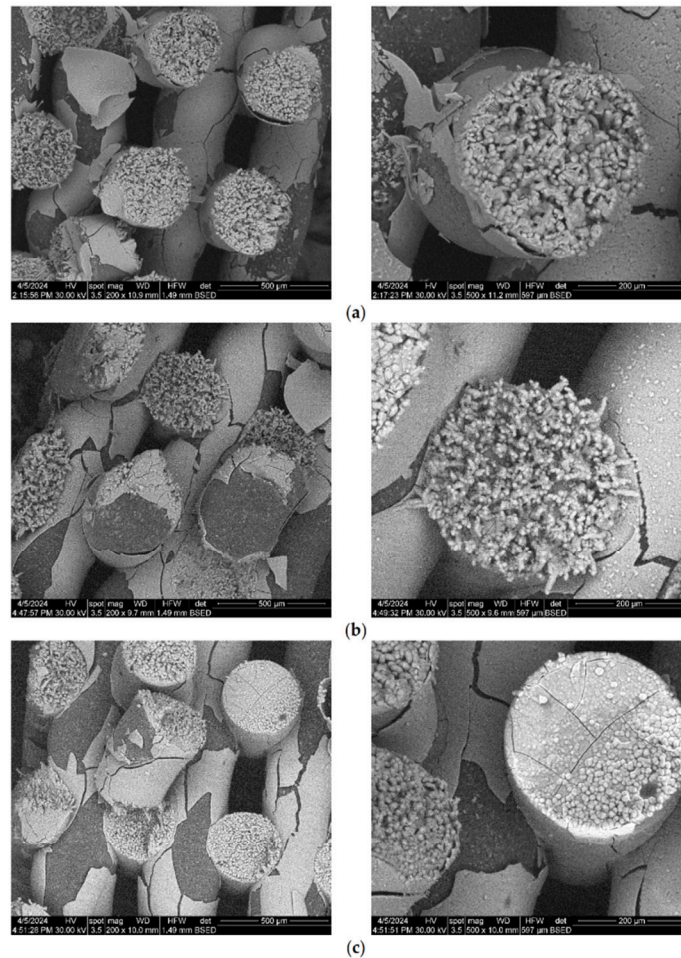

(**a**)

(**b**)
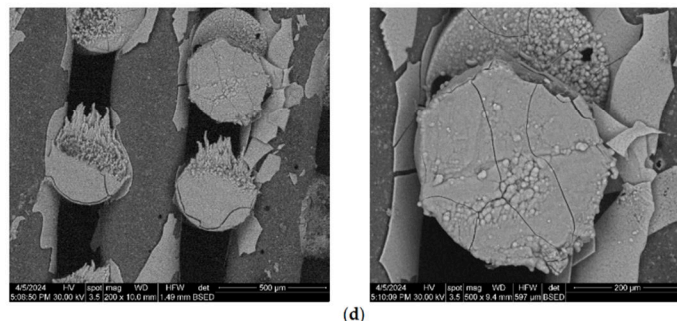

(**c**)

Figure 16. *Cont.*

(**d**)

Figure 16. SEM images of the 3D-printed composite scaffolds containing hydrothermal-obtained SrHA after 28 days of immersion in SBF: (**a**) PCL-HAHT-Sr1%, (**b**) PCL-HAHT-Sr5%, (**c**) PCL-HAHT-Sr10%, (**d**) PCL-HAHT-Sr20%.

3.6. Biological In Vitro Scaffold Performance

In order to assess the biocompatibility of the different types of 3D-printed scaffolds, the F-actin staining of MC3T3-E1 cells attached on the surface of these materials was performed. The images shown in Figure 17 revealed a good adhesion of these cells for all types of scaffolds tested, being distributed within the whole surface of them after 24 h of incubation. A good cytocompatibility was noticed for PCL sample (Figure 17a), as it was previously reported [27]. In the case of samples containing SrHA obtained by precipitation, the best cell morphology was achieved for Sr1, 5, and 10 (Figure 17b). For HAHT-based samples, the addition of Sr increases the cell attachment compared to PCL-HAHT scaffold (Figure 17c). The analysis of images captured at a higher magnification indicated a higher cell density for PCL-HAPR, PCL-HAPR-Sr1, 5, and 10, being observed an organized actin filaments network with numerous cell-to-cell junctions, which suggest a functional osteoblast phenotype. In addition, a good cell interaction was shown for PCL-HAHT-Sr30.

Relative cell adhesion was investigated for all the samples using images of fluorescence microscopy. Images were analyzed quantitatively with the help of ImageJ and results were presented as average cell number (Figure 18). In the case of composites containing precipitation-obtained SrHA, results are higher for lower Sr concentrations, while in the case of hydrothermal-obtained samples, better results are obtained at higher concentrations, apart from PCL–HAHT-Sr20%. Although pristine PCL scaffolds also had good results, in confirming the biocompatible nature of this polymer and its suitability in developing new composite materials, it is often considered that the improvement brought by the added HA/SrHA is more visible on longer periods of time [27].

The good cytocompatibility of all scaffolds was confirmed by the metabolic activity of MC3T3-E1 osteoblasts measured by MTT assay (Figure 19a), manifesting no important differences between the samples. However, the lowest values were noticed in the case of Sr20, for both types of HA. Furthermore, the biological evaluation included the examination of the cells attached to the plastic surface of the culture dish, under the scaffold. The F-actin staining revealed a high attachment of pre-osteoblasts (Figure S3 from Supporting Information), not being disturbed by the materials, confirming their biocompatibility for the neighboring cells in the case of tissue engineering application. Moreover, the NO level was unchanged compared to control cells (not exposed to materials), suggesting that the scaffolds did not induce inflammation (Figure 19b). In the case of LDH release, the highest level was obtained after the incubation with PCL-HAPR-Sr20, being in agreement with the results of MTT assay (Figure 19a) and F-actin staining (Figure 17). In this case, the decreased attachment could be correlated with a loss in cell membrane integrity.

30
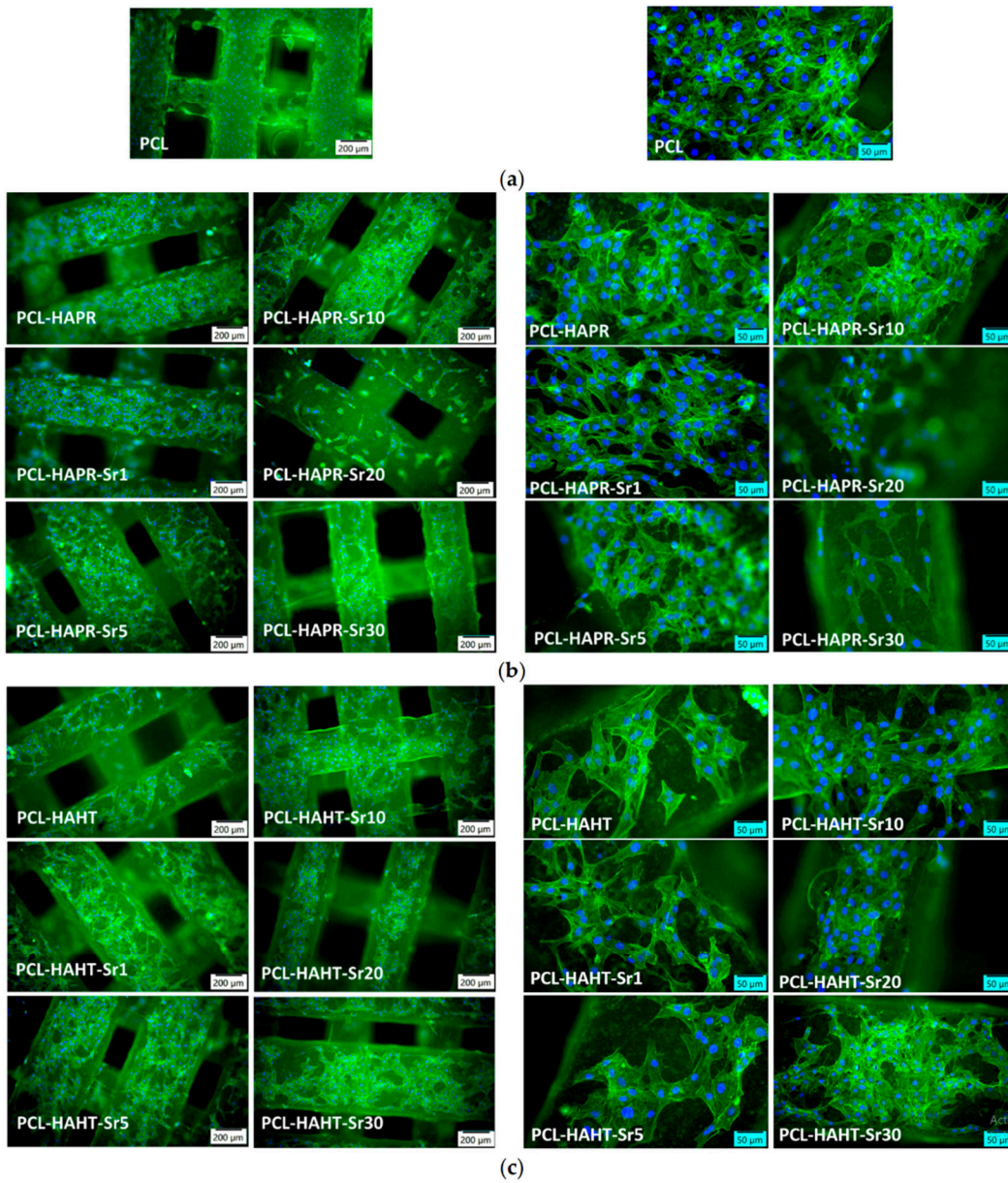
Figure 17. Representative images of fluorescence microscopy with different magnifications after 24 h of incubation showing the actin cytoskeleton staining in MC3T3-E1 pre-osteoblasts attached on the surface of 3D-printed scaffolds: (**a**) containing only PCL, (**b**) containing precipitation-obtained SrHA (**c**) containing hydrothermal-obtained SrHA. F-actin was stained in green with phalloidin-FITC and nuclei in blue with DAPI.

31
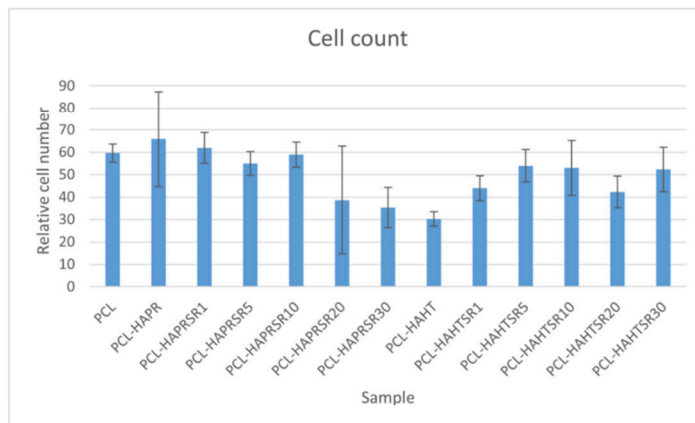
Figure 18. Quantitative analysis of cell adhesion on the scaffolds after 24 h of incubation. Results are represented as mean $\pm$ SD (n = 3).
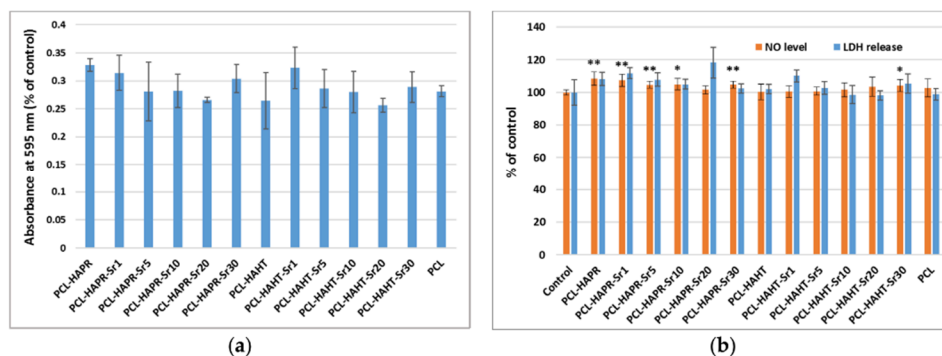
Figure 19. Biocompatibility evaluation of 3D-printed scaffolds, containing PCL and HA/SrHA obtained by precipitation and hydrothermal method, after 24 h of incubation with MC3T3-E1 pre-osteoblasts by measuring the viability of cells attached on these scaffolds: (**a**) cell viability was assessed by MTT assay and represented as mean $\pm$ SD (n = 2); (**b**) NO level and LDH release in culture medium. The results were calculated as mean $\pm$ SD (n = 3) and expressed relative to control (cells incubated without scaffolds) for NO and LDH assays (* $p < 0.05$ and ** $p < 0.01$ compared to control).

4. Conclusions

PCL 70% (wt.)–HA/SrHA 30% (wt.) composite materials were obtained through melt-blending and used for the 3D printing of scaffolds through the FDM technique. Melt-blending is simple, cost-efficient, and avoids cytotoxicity associated with solvent residuals. The FDM technique is simple to use, reliable, and capable of putting into practice complex designs. Three-dimensional scaffold design was suited for overall biological performance due to adequate strand arrangement, layer thickness, and porosity. Experimental results indicate that the obtained 3D scaffolds favor the adhesion and proliferation of pre-osteoblasts attached to these surfaces, avoiding drawbacks associated with poor integration of scaffolds due to their low interaction with cells.

Overall good results were obtained, although in the case of F-actin staining, the best cell morphology was achieved for lower Sr concentrations, and subsequently, in the case

of LDH release, the highest level was obtained after the incubation with PCL-HAPR-Sr20, being in agreement with the results of MTT assay and F-actin staining. The decreased attachment could be correlated with a loss in cell membrane integrity. Based on cell viability, quantitative analysis of cell adhesion and mechanical properties, we consider that samples containing SrHA with a lower concentration of Sr are better suited for bone tissue applications. Also, comparing the overall results between the scaffolds containing HA/SrHA obtained via different synthesis methods, we consider that the precipitation method is recommended. The precipitation method has the additional advantages of being more simple, easy, less expensive, and as previously shown [23], a more amorphous structure and a carbonated composition, capable of integrating better in the host tissue due to similarities with the natural-occurring apatite.

The manufacturing strategy applied in this study may be used for the development of more complex and patient-specific substitutes, allowing the inclusion of additional bioactive substances into these composites that better match the patient-specific needs of the native bone tissue. It is expected that similar strategies can become widely used and, thus, evolve as a next-generation medical device for managing osteoporosis fractures or even other bone defects.

Supplementary Materials: The following supporting information can be downloaded at: https://www.mdpi.com/article/10.3390/polym16111511/s1, Figure S1: EDS mapping and spectra of all composite scaffolds; Figure S2: Cross-section SEM images of PCL-HAHT-Sr5% composite scaffold highlighting the thickness of the apatite covering layer; Figure S3: Representative fluorescence images of F-actin staining in MC3T3-E1 osteoblasts attached on the surface of tissue culture dish, under the 3D-printed scaffolds, after 24 h of incubation (green: actin filaments, blue: nuclei, objective magnification 16×). The control without any scaffold was represented by cells grown on the plastic surface of culture dish.

Author Contributions: Conceptualization, C.I.C., V.L.E. and A.F.; methodology, C.I.C., V.L.E. and A.F.; software, C.I.C.; formal analysis, C.I.C., D.L., V.L.E., A.I.N. and M.S.S.; data curation, V.L.E., D.F. and A.F.; writing—original draft preparation, C.I.C., V.L.E. and M.S.S.; writing—review and editing, C.I.C., V.L.E., D.F. and A.F. All authors have read and agreed to the published version of the manuscript.

Data Availability Statement: Data are contained within the article and the Supplementary Materials.

Conflicts of Interest: The authors declare no conflicts of interest.

References

1. Dumitrescu, C.R.; Neacsu, I.A.; Surdu, V.A.; Nicoara, A.I.; Codrea, C.I.; Pop, C.E.; Trusca, R.; Andronescu, E. Maturation of Hydroxyapatite from Biogenic Calcium Source—A Comparative Study. *U.P.B. Sci. Bull. Ser. B* **2022**, *84*, 21–30.
2. Ashrafi, M.; Ghalichi, F.; Mirzakouchaki, B.; Doblare, M. On the Effect of Antiresorptive Drugs on the Bone Remodeling of the Mandible after Dental Implantation: A Mathematical Model. *Sci. Rep.* **2021**, *11*, 2792. [CrossRef]
3. Dumitrescu, C.R.; Neacsu, I.A.; Surdu, V.A.; Nicoara, A.I.; Iordache, F.; Trusca, R.; Ciocan, L.T.; Ficai, A.; Andronescu, E. Nano-Hydroxyapatite vs. Xenografts: Synthesis, Characterization, and In Vitro Behavior. *Nanomaterials* **2021**, *11*, 2289. [CrossRef] [PubMed]
4. Custodio, C.L.; Broñola, P.J.M.; Cayabyab, S.R.; Lagura, V.U.; Celorico, J.R.; Basilia, B.A. Powder Loading Effects on the Physicochemical and Mechanical Properties of 3D Printed Poly Lactic Acid/Hydroxyapatite Biocomposites. *Int. J. Bioprint* **2021**, *7*, 326. [CrossRef] [PubMed]
5. Lin, K.; Chang, J. 1—Structure and Properties of Hydroxyapatite for Biomedical Applications. In *Hydroxyapatite (Hap) for Biomedical Applications*; Mucalo, M., Ed.; Woodhead Publishing: Cambridge, UK, 2015; pp. 3–19. [CrossRef]
6. Zhu, T.; Li, J.; Cui, L.; Zhang, Z.; Zhuang, X.; Ding, J. Poly(Lactic-Co-Glycolic Acid)-Based Composite Bone-Substitute Materials. *Bioact. Mater.* **2021**, *6*, 346–360. [CrossRef] [PubMed]
7. Jakus, A.E.; Rutz, A.L.; Jordan, S.W.; Kannan, A.; Mitchell, S.M.; Yun, C.; Koube, K.D.; Yoo, S.C.; Whiteley, H.E.; Richter, C.-P.; et al. Hyperelastic "Bone": A Highly Versatile, Growth Factor–Free, Osteoregenerative, Scalable, and Surgically Friendly Biomaterial. *Sci. Transl. Med.* **2016**, *8*, 358ra127. [CrossRef] [PubMed]

8. Zhu, L.; Luo, D.; Liu, Y. Effect of the Nano/Microscale Structure of Biomaterial Scaffolds on Bone Regeneration. *Int. J. Oral Sci.* **2020**, *12*, 6. [CrossRef] [PubMed]

9. Babilotte, J.; Martin, B.; Guduric, V.; Bareille, R.; Agniel, R.; Roques, S.; Héroguez, V.; Dussauze, M.; Gaudon, M.; Le Nihouannen, D.; et al. Development and Characterization of a PLGA-HA Composite Material to Fabricate 3D-Printed Scaffolds for Bone Tissue Engineering. *Mater. Sci. Eng. C* **2021**, *118*, 111334. [CrossRef] [PubMed]

10. Codrea, C.I.; Croitoru, A.-M.; Baciu, C.C.; Melinescu, A.; Ficai, D.; Fruth, V.; Ficai, A. Advances in Osteoporotic Bone Tissue Engineering. *J. Clin. Med.* **2021**, *10*, 253. [CrossRef]

11. Eiden-Aßmann, S.; Viertelhaus, M.; Heiß, A.; Hoetzer, K.A.; Felsche, J. The Influence of Amino Acids on the Biomineralization of Hydroxyapatite in Gelatin. *J. Inorg. Biochem.* **2002**, *91*, 481–486. [CrossRef]

12. Seyedsalehi, A.; Daneshmandi, L.; Barajaa, M.; Riordan, J.; Laurencin, C.T. Fabrication and Characterization of Mechanically Competent 3D Printed Polycaprolactone-Reduced Graphene Oxide Scaffolds. *Sci. Rep.* **2020**, *10*, 22210. [CrossRef]

13. Zimmerling, A.; Yazdanpanah, Z.; Cooper, D.M.L.; Johnston, J.D.; Chen, X. 3D Printing PCL/nHA Bone Scaffolds: Exploring the Influence of Material Synthesis Techniques. *Biomater. Res.* **2021**, *25*, 3. [CrossRef] [PubMed]

14. Neacsu, I.A.; Matei, L.; Birca, A.C.; Nicoara, A.I.; Ene, V.L.; Dragu, L.D.; Ficai, A.; Bleotu, C.; Andronescu, E. Curcumin—Hydroxyapatite Systems Used for Bone Cancer Treatment. *Rev. Romana Mater./Rom. J. Mater.* **2021**, *51*, 505–513.

15. Boccaccio, A. Design of Materials for Bone Tissue Scaffolds. *Materials* **2021**, *14*, 5985. [CrossRef]

16. Nicoara, A.I.; Neacsu, I.A.; Ene, V.L.; Vasile, B.S.; Ficai, A.; Andronescu, E. Hydroxyapatite/Carbon Based Biocomposite Scaffolds as Prospective Materials for Bone Tissue Engineering. *UPB Sci. Bull. Ser. B Chem. Mater. Sci.* **2019**, *81*, 107–120.

17. Barba, A.; Maazouz, Y.; Diez-Escudero, A.; Rappe, K.; Espanol, M.; Montufar, E.B.; Öhman-Mägi, C.; Persson, C.; Fontecha, P.; Manzanares, M.-C.; et al. Osteogenesis by Foamed and 3D-Printed Nanostructured Calcium Phosphate Scaffolds: Effect of Pore Architecture. *Acta Biomater.* **2018**, *79*, 135–147. [CrossRef] [PubMed]

18. Gao, X.; Yu, N.; Li, J. Influence of Printing Parameters and Filament Quality on Structure and Properties of Polymer Composite Components Used in the Fields of Automotive. In *Structure and Properties of Additive Manufactured Polymer Components*; Friedrich, K., Walter, R., Soutis, C., Advani, S.G., Fiedler, I., Habil, B., Eds.; Woodhead Publishing: Cambridge, UK, 2020; pp. 303–330. [CrossRef]

19. Percoco, G.; Uva, A.E.; Fiorentino, M.; Gattullo, M.; Manghisi, V.M.; Boccaccio, A. Mechanobiological Approach to Design and Optimize Bone Tissue Scaffolds 3D Printed with Fused Deposition Modeling: A Feasibility Study. *Materials* **2020**, *13*, 648. [CrossRef]

20. Zhang, S.; Dong, Y.; Chen, M.; Xu, Y.; Ping, J.; Chen, W.; Liang, W. Recent Developments in Strontium-Based Biocomposites for Bone Regeneration. *J. Artif. Organs* **2020**, *23*, 191–202. [CrossRef] [PubMed]

21. Weng, L.; Teusink, M.J.; Shuler, F.D.; Parecki, V.; Xie, J. Highly Controlled Coating of Strontium-Doped Hydroxyapatite on Electrospun Poly(ε-Caprolactone) Fibers. *J. Biomed. Mater. Res. Part B Appl. Biomater.* **2017**, *105*, 753–763. [CrossRef]

22. Wang, Z.; Wang, Y.; Yan, J.; Zhang, K.; Lin, F.; Xiang, L.; Deng, L.; Guan, Z.; Cui, W.; Zhang, H. Pharmaceutical Electrospinning and 3D Printing Scaffold Design for Bone Regeneration. *Adv. Drug Deliv. Rev.* **2021**, *174*, 504–534. [CrossRef]

23. Codrea, C.I.; Lincu, D.; Atkinson, I.; Culita, D.C.; Croitoru, A.-M.; Dolete, G.; Trusca, R.; Vasile, B.S.; Stan, M.S.; Ficai, D.; et al. Comparison between Two Different Synthesis Methods of Strontium-Doped Hydroxyapatite Designed for Osteoporotic Bone Restoration. *Materials* **2024**, *17*, 1472. [CrossRef] [PubMed]

24. Pierantozzi, D.; Scalzone, A.; Jindal, S.; Stīpniece, L.; Šalma-Ancāne, K.; Dalgarno, K.; Gentile, P.; Mancuso, E. 3D Printed Sr-Containing Composite Scaffolds: Effect of Structural Design and Material Formulation towards New Strategies for Bone Tissue Engineering. *Compos. Sci. Technol.* **2020**, *191*, 108069. [CrossRef]

25. Wang, F.; Tankus, E.B.; Santarella, F.; Rohr, N.; Sharma, N.; Märtin, S.; Michalscheck, M.; Maintz, M.; Cao, S.; Thieringer, F.M. Fabrication and Characterization of PCL/HA Filament as a 3D Printing Material Using Thermal Extrusion Technology for Bone Tissue Engineering. *Polymers* **2022**, *14*, 669. [CrossRef] [PubMed]

26. Gerdes, S.; Mostafavi, A.; Ramesh, S.; Memic, A.; Rivero, I.V.; Rao, P.; Tamayol, A. Process–Structure–Quality Relationships of Three-Dimensional Printed Poly(Caprolactone)-Hydroxyapatite Scaffolds. *Tissue Eng. Part A* **2020**, *26*, 279–291. [CrossRef] [PubMed]

27. Rezania, N.; Asadi-Eydivand, M.; Abolfathi, N.; Bonakdar, S.; Mehrjoo, M.; Solati-Hashjin, M. Three-Dimensional Printing of Polycaprolactone/Hydroxyapatite Bone Tissue Engineering Scaffolds Mechanical Properties and Biological Behavior. *J. Mater. Sci. Mater. Med.* **2022**, *33*, 31. [CrossRef] [PubMed]

28. Dias, J.R.; Sousa, A.; Augusto, A.; Bártolo, P.J.; Granja, P.L. Electrospun Polycaprolactone (PCL) Degradation: An In Vitro and In Vivo Study. *Polymers* **2022**, *14*, 3397. [CrossRef]

29. Kokubo, T.; Takadama, H. How Useful Is SBF in Predicting in Vivo Bone Bioactivity? *Biomaterials* **2006**, *27*, 2907–2915. [CrossRef] [PubMed]

30. de Oliveira Junior, J.M.; Montagner, P.G.; Carrijo, R.C.; Martinez, E.F. Physical Characterization of Biphasic Bioceramic Materials with Different Granulation Sizes and Their Influence on Bone Repair and Inflammation in Rat Calvaria. *Sci. Rep.* **2021**, *11*, 4484. [CrossRef]

31. Mancuso, E.; Shah, L.; Jindal, S.; Serenelli, C.; Tsikriteas, Z.M.; Khanbareh, H.; Tirella, A. Additively Manufactured BaTiO3 Composite Scaffolds: A Novel Strategy for Load Bearing Bone Tissue Engineering Applications. *Mater. Sci. Eng. C* **2021**, *126*, 112192. [CrossRef]

32. Porta, M.; Tonda-Turo, C.; Pierantozzi, D.; Ciardelli, G.; Mancuso, E. Towards 3D Multi-Layer Scaffolds for Periodontal Tissue Engineering Applications: Addressing Manufacturing and Architectural Challenges. *Polymers* **2020**, *12*, 2233. [CrossRef]

33. Jakus, A.E.; Geisendorfer, N.R.; Lewis, P.L.; Shah, R.N. 3D-Printing Porosity: A New Approach to Creating Elevated Porosity Materials and Structures. *Acta Biomater.* **2018**, *72*, 94–109. [CrossRef] [PubMed]

34. Bružauskaitė, I.; Bironaitė, D.; Bagdonas, E.; Bernotienė, E. Scaffolds and Cells for Tissue Regeneration: Different Scaffold Pore Sizes—Different Cell Effects. *Cytotechnology* **2016**, *68*, 355–369. [CrossRef] [PubMed]

35. Jiang, W.; Shi, J.; Li, W.; Sun, K. Morphology, Wettability, and Mechanical Properties of Polycaprolactone/Hydroxyapatite Composite Scaffolds with Interconnected Pore Structures Fabricated by a Mini-Deposition System. *Polym. Eng. Sci.* **2012**, *52*, 2396–2402. [CrossRef]

36. Dobriţa, C.-I.; Bădănoiu, A.-I.; Voicu, G.; Nicoară, A.-I.; Dumitru, S.-M.; Puşcaşu, M.-E.; Chiriac, Ş.; Ene, R.; Iordache, F. Porous Bioceramic Scaffolds Based on Akermanite Obtained by 3D Printing for Bone Tissue Engineering. *Ceram. Int.* **2023**, *49*, 35898–35906. [CrossRef]

37. Stafin, K.; Śliwa, P.; Piątkowski, M. Towards Polycaprolactone-Based Scaffolds for Alveolar Bone Tissue Engineering: A Biomimetic Approach in a 3D Printing Technique. *Int. J. Mol. Sci.* **2023**, *24*, 16180. [CrossRef] [PubMed]

38. Gonçalves, E.M.; Oliveira, F.J.; Silva, R.F.; Neto, M.A.; Fernandes, M.H.; Amaral, M.; Vallet-Regí, M.; Vila, M. Three-Dimensional Printed PCL-Hydroxyapatite Scaffolds Filled with CNTs for Bone Cell Growth Stimulation. *J. Biomed. Mater. Res. Part B Appl. Biomater.* **2016**, *104*, 1210–1219. [CrossRef] [PubMed]

39. Qi, X.; Pei, P.; Zhu, M.; Du, X.; Xin, C.; Zhao, S.; Li, X.; Zhu, Y. Three Dimensional Printing of Calcium Sulfate and Mesoporous Bioactive Glass Scaffolds for Improving Bone Regeneration in Vitro and in Vivo. *Sci. Rep.* **2017**, *7*, 42556. [CrossRef] [PubMed]

40. Suganthi, R.V.; Prakash Parthiban, S.; Elayaraja, K.; Girija, E.K.; Kulariya, P.; Katharria, Y.S.; Singh, F.; Asokan, K.; Kanjilal, D.; Narayana Kalkura, S. Investigations on the in Vitro Bioactivity of Swift Heavy Oxygen Ion Irradiated Hydroxyapatite. *J. Mater. Sci. Mater. Med.* **2009**, *20*, 271–275. [CrossRef]

41. Rajzer, I.; Rom, M.; Menaszek, E.; Fabia, J.; Kwiatkowski, R. Conductive Polyaniline Patterns on Electrospun Polycaprolactone/Hydroxyapatite Scaffolds for Bone Tissue Engineering. *Materials* **2021**, *14*, 4837. [CrossRef]

35

Chapter 7: General conclusions and perspectives

The main goals of this thesis were the developing and characterization of multi-layered 3D printed composite scaffolds for bone tissue engineering applications comprised of 70% wt. PCL and 30% wt. SrHA through FDM technique, as well as 10% w/v GelMA and 5% w/v SrHA through DLP technique, both with different Sr concentrations. Based on the synthesis method, two types of SrHA were obtained, through precipitation (PR) and hydrothermal conditions (HT), respectively. This enables us to compare the two methods to create a more thorough understanding of the influence synthesis has on the proprieties of the composite scaffolds. Each constituent of the composite scaffolds underwent extensive characterization.

The synthesized HA/SrHA powders were characterized for chemical composition, crystallinity, and morphology using EDX, XRD, SEM, and TEM, respectively. Both synthesis protocols successfully produced HA exhibiting Ca:P ratios alike to the stoichiometric value of 1.67. PR obtained HA displayed a round shape, while HT obtained HA exhibited a rod-shape morphology. SrHA was integrated in the PCL matrix to form the composite used for obtaining 3D scaffolds. PCL – SrHA scaffolds were fabricated via EnvisionTEC's 3D Bioplotter pressure-assisted technology, incorporating both PR-obtained and HT-obtained HA/SrHA at concentration of ±30% w/w., featuring a circular shape with a square grid pattern, a strand diameter of 360 μm, and 600 μm between strands, with 8 layers. The printing process underwent optimization to achieve layered structures with open porosity. The composite 3D-printed PCL – HA/SrHA scaffolds were thoroughly characterized. TG analysis was employed to evaluate the percentage of inorganic and organic components of the composites. SEM was employed to observe the morpho-structural details of the scaffold surface and cross-section, providing insights into their microstructure and porosity. Visual analyses of SEM images revealed similar dispersion of HA/SrHA within PCL. The mechanical characteristics of the scaffolds were evaluated to ensure alignment with the expected forces that genuine bone must withstand during normal function. Chemical bioactivity evaluation was conducted to determine the scaffolds' capacity to interact and satisfyingly blend into genuine bone tissue. Finally, cytotoxicity examination was performed

to evaluate the scaffolds' biocompatibility and capability to avoid adverse reactions, ensuring their safety in bone tissue engineering applications. Compressive tests conducted on composite scaffolds revealed overall similar values with the ones for PCL-based porous scaffolds. Specifically, small differences were observed between scaffolds containing PR-obtained and HT-obtained HA/SrHA. Overall, PR-obtained SrHA performed better. These distinctions were attributed to inherent characteristics of the ceramic component.

SrHA was also used to fabricate GelMA – HA/SrHA composite scaffolds through DLP 3D printing. Photocurable GelMA with an approximative degree of substitution, of 75.4% degrees of methacryloylation was synthesized from gelatin from porcine skin (type A) and methacrylic anhydride at different concentrations. 10% w/v GelMA and 5% w/v SrHA mixtures were then photocured using Lithium phenyl-2,4,6-trimethylbenzoyl phosphinate (LAP) as a photoinitiator and a UV light source at 405 nm and 12 mW/cm^2 to obtain photo-polymerized gels. Mechanical properties of hydrogel composites were observed to improve by adding SrHA. The resulting cross-linked composites were analyzed for chemical composition using FTIR spectroscopy to confirm successful crosslinking. Additionally, their external structure and morphology were assessed via SEM. Swelling analyses were conducted on freeze-dried GelMA-based composite scaffolds, demonstrating decreased swelling rate. Swelling capability assessments of freeze-dried GelMA-based composite exhibited lower swelling percentages compared to pristine GelMA. Structural and morphological analyses of GelMA-based composite scaffolds were conducted using TG, SEM, revealing differences correlated with the category and concentration of HA/SrHA within the composites.

One potential approach to improving mechanical and chemical properties of hydrogels is to incorporate a ceramic component, taking advantage of ceramics' biocompatibility, corrosion resistance, and favorable compressive modulus. Future endeavors will explore the creation of GelMA – SrHA scaffolds with different SrHA content. The resulting products must undergo analysis encompassing mechanical properties, internal and external structures, as well as swelling and degradation behaviors. Moreover,

new 3D printed composite scaffolds can be generated by exploring alternative crosslinking methods. This approach could facilitate the creation of structures with more precise shapes and customizable mechanical properties.

Challenges and future research directions for various medical 3D applications include enhancing printing resolution, speed, and repeatability in tissue engineering, as well as increasing cell interactions and migration in regenerative medicine. For engineered tissue replicas, integrating neural and vascular structures is crucial. The creation of entirely functional, common-size organs necessitates combining cell printing with other biofabrication techniques.

All the Sr-containing biomaterials, obtained in this study, displayed superior properties compared to their Sr-free analogs. Therefore, the designed scaffolds highlighted encouraging prospectives for SrHA-based materials with antiosteoporosis activity. The results may encourage this research direction to the future phase by carrying out *in vivo* tests to evidence the safe usage of these materials as a local source of Sr in the defected bone sites. The 3D design and printing of scaffolds can further the management of various bone diseases in an individualized way. A release profile of an active substance could be adapted to the needs of the patient. Also, the scaffold macroscopic form and mechanical performances can be adapted to the type of bone tissue to be restored. We also consider that the fabricated scaffolds meet the key indicators for the effective use of biodegradable scaffolds which include high porosity, a completely interconnected pore structure, and a gradual degradation rate of the biomaterial[18].

In summary, this study illustrates the feasibility of designing 3D composite scaffolds containing strontium using various materials and fabrication technologies. This approach allows for the manufacturing of composite structures with finely tuned properties by adjusting scaffold design, chosen materials and concentration, crosslinking methods and degrees. The composite scaffolds produced in this study show great promise for tissue engineering applications, particularly in cases requiring the repair and regeneration of bone, but have potential for interfaces between different tissues, such as in osteochondral tissue engineering.

Chapter 8: List of publications and participations on national conferences

Published articles included in the thesis (main author)

a) Review article:

1. **Codrea, C.I**.; Croitoru, A.-M.; Baciu, C.C.; Melinescu, A.; Ficai, D.; Fruth, V.; Ficai, A. Advances in Osteoporotic Bone Tissue Engineering. Journal of Clinical Medicine 2021, 10, 253. https://doi.org/10.3390/jcm10020253 (IF - 4.242 - Q1);

b) Original research articles:

2. **Codrea, C.I**.; Lincu, D.; Atkinson, I.; Culita, D.C.; Croitoru, A.-M.; Dolete, G.; Trusca, R.; Vasile, B.S.; Stan, M.S.; Ficai, D.; et al. Comparison between Two Different Synthesis Methods of Strontium-Doped Hydroxyapatite Designed for Osteoporotic Bone Restoration. *Materials* 2024, *17*, 1472. https://doi.org/10.3390/ma17071472 (IF - 3.4 - Q2);

3. **Codrea, C.I**.; Lincu, D.; Ene, V.L.; Nicoară, A.I.; Stan, M.S.; Ficai, D.; Ficai, A. Three-Dimensional-Printed Composite Scaffolds Containing Poly-ε-Caprolactone and Strontium-Doped Hydroxyapatite for Osteoporotic Bone Restoration. *Polymers* 2024, *16*, 1511. https://doi.org/10.3390/polym16111511 (IF - 4.7 - Q1);

4. **Codrea, C.I.,** Baykara, D.; Mitran, R.-A.; Koyuncu, A.C.Ç.; Gunduz, O.; Ficai, A. 3D-Bioprinted Gelatin Methacryloyl-Strontium-Doped Hydroxyapatite Composite Hydrogels Scaffolds for Bone Tissue Regeneration. *Polymers* 2024, *16*, 1932. https://doi.org/10.3390/polym16131932, (IF - 4.7 - Q1).

IF cumulative: 4.242 + 3.4 + 4.7 + 4.7 = 17,042

Published articles related to the thesis (co-author):

1. Cristina Dumitrescu, Ionela Neacsu, Vasile Surdu, Adrian Nicoara, **Cosmin Codrea**, Cristian Pop, Roxana Trusca, Ecaterina Andronescu; Maturation of hydroxyapatite from biogenic calcium source – a comparative study; Scientific Bulletin of University Politehnica of Bucharest, Series B, Vol. 84, Iss. 1, 2022 (IF – 0.5 - Q4).

Conference participations related to the thesis:

1. **Cosmin Iulian Codrea,** Daniel Lincu, Irina Atkinson, Alexa Maria Croitoru, Bogdan Stefan Vasile, Adrian Ionut, Nicoară, Vladimir Lucian Ene, Miruna Silvia Stan, Anton Ficai - **3D-Printed Scaffolds for Osteoporotic Bone Restoration based on Poly-ε-Caprolactone and Strontium-Doped Hydroxyapatite,** Applications of Chemistry in Nanosciences and Biomaterials Engineering – NanoBioMat 2024, 19-21 June 2024.

Bibliography

(1) Duda, G. N.; Geissler, S.; Checa, S.; Tsitsilonis, S.; Petersen, A.; Schmidt-Bleek, K. The Decisive Early Phase of Bone Regeneration. *Nature Reviews Rheumatology* **2023**, *19* (2), 78–95. https://doi.org/10.1038/s41584-022-00887-0.

(2) Xie, Y.; Zhang, L.; Xiong, Q.; Gao, Y.; Ge, W.; Tang, P. Bench-to-Bedside Strategies for Osteoporotic Fracture: From Osteoimmunology to Mechanosensation. *Bone Research* **2019**, *7* (1), 25. https://doi.org/10.1038/s41413-019-0066-7.

(3) Sterling, J. A.; Guelcher, S. A. Biomaterial Scaffolds for Treating Osteoporotic Bone. *Current Osteoporosis Reports* **2014**, *12* (1), 48–54. https://doi.org/10.1007/s11914-014-0187-2.

(4) Lehman, R. A. J.; Kang, D. G.; Wagner, S. C. Management of Osteoporosis in Spine Surgery. *JAAOS - Journal of the American Academy of Orthopaedic Surgeons* **2015**, *23* (4).

(5) Wei, H.; Cui, J.; Lin, K.; Xie, J.; Wang, X. Recent Advances in Smart Stimuli-Responsive Biomaterials for Bone Therapeutics and Regeneration. *Bone Research* **2022**, *10* (1), 17. https://doi.org/10.1038/s41413-021-00180-y.

(6) Yazdanpanah, Z.; Sharma, N. K.; Raquin, A.; Cooper, D. M. L.; Chen, X.; Johnston, J. D. Printing Tissue-Engineered Scaffolds Made of Polycaprolactone and Nano-Hydroxyapatite with Mechanical Properties Appropriate for Trabecular Bone Substitutes. *BioMedical Engineering OnLine* **2023**, *22* (1), 73. https://doi.org/10.1186/s12938-023-01135-6.

(7) Gordon, A.; Newsome, F.; Ahern, D. P.; McDonnell, J. M.; Cunniffe, G.; Butler, J. S. Iliac Crest Bone Graft versus Cell-Based Grafts to Augment Spinal Fusion: A Systematic Review and Meta-Analysis. *European Spine Journal* **2024**, *33* (1), 253–263. https://doi.org/10.1007/s00586-023-07941-9.

(8) Humbert, P.; Kampleitner, C.; De Lima, J.; Brennan, M. Á.; Lodoso-Torrecilla, I.; Sadowska, J. M.; Blanchard, F.; Canal, C.; Ginebra, M.-P.; Hoffmann, O.; Layrolle, P. Phase Composition of Calcium Phosphate Materials Affects Bone Formation by Modulating Osteoclastogenesis. *Acta Biomaterialia* **2024**, *176*, 417–431. https://doi.org/10.1016/j.actbio.2024.01.022.

(9) Schulze, F.; Lang, A.; Schoon, J.; Wassilew, G. I.; Reichert, J. Scaffold Guided Bone Regeneration for the Treatment of Large Segmental Defects in Long Bones. *Biomedicines* **2023**, *11* (2). https://doi.org/10.3390/biomedicines11020325.

(10) Zhang, S.; Dong, Y.; Chen, M.; Xu, Y.; Ping, J.; Chen, W.; Liang, W. Recent Developments in Strontium-Based Biocomposites for Bone Regeneration. *Journal of Artificial Organs* **2020**, *23* (3), 191–202. https://doi.org/10.1007/s10047-020-01159-y.

(11) Frasnelli, M.; Cristofaro, F.; Sglavo, V. M.; Dirè, S.; Callone, E.; Ceccato, R.; Bruni, G.; Cornaglia, A. I.; Visai, L. Synthesis and Characterization of Strontium-Substituted Hydroxyapatite Nanoparticles for Bone Regeneration. *Materials Science and Engineering: C* **2017**, *71*, 653–662. https://doi.org/10.1016/j.msec.2016.10.047.

(12) Tao, Z.-S.; Zhou, W.-S.; He, X.-W.; Liu, W.; Bai, B.-L.; Zhou, Q.; Huang, Z.-L.; Tu, K.; Li, H.; Sun, T.; Lv, Y.-X.; Cui, W.; Yang, L. A Comparative Study of Zinc, Magnesium, Strontium-Incorporated Hydroxyapatite-Coated Titanium Implants for Osseointegration of Osteopenic Rats. *Materials Science and Engineering: C* **2016**, *62*, 226–232. https://doi.org/10.1016/j.msec.2016.01.034.

(13) Anandan, D.; Jaiswal, A. K. Synthesis Methods of Hydroxyapatite and Biomedical Applications: An Updated Review. *Journal of the Australian Ceramic Society* **2024**, *60* (2), 663–679. https://doi.org/10.1007/s41779-023-00943-2.

(14) Pierantozzi, D.; Scalzone, A.; Jindal, S.; Stīpniece, L.; Šalma-Ancāne, K.; Dalgarno, K.; Gentile, P.; Mancuso, E. 3D Printed Sr-Containing Composite Scaffolds: Effect of Structural Design and Material Formulation towards New Strategies for Bone Tissue Engineering. *Composites Science and Technology* **2020**, *191*, 108069. https://doi.org/10.1016/j.compscitech.2020.108069.

(15) You, J.; Zhang, Y.; Zhou, Y. Strontium Functionalized in Biomaterials for Bone Tissue Engineering: A Prominent Role in Osteoimmunomodulation. *Frontiers in Bioengineering and Biotechnology* **2022**, *10*.

(16) Melnik, E. V.; Shkarina, S. N.; Ivlev, S. I.; Weinhardt, V.; Baumbach, T.; Chaikina, M. V.; Surmeneva, M. A.; Surmenev, R. A. In Vitro Degradation Behaviour of Hybrid Electrospun Scaffolds of Polycaprolactone and Strontium-Containing Hydroxyapatite Microparticles. *Polymer Degradation and Stability* **2019**, *167*, 21–32. https://doi.org/10.1016/j.polymdegradstab.2019.06.017.

(17) Shuai, C.; Yang, W.; Feng, P.; Peng, S.; Pan, H. Accelerated Degradation of HAP/PLLA Bone Scaffold by PGA Blending Facilitates Bioactivity and Osteoconductivity. *Bioactive Materials* **2021**, *6* (2), 490–502. https://doi.org/10.1016/j.bioactmat.2020.09.001.

(18) Laubach, M.; Herath, B.; Bock, N.; Suresh, S.; Saifzadeh, S.; Dargaville, B. L.; McGovern, J.; Wille, M.-L.; Hutmacher, D. W.; Medeiros Savi, F. In Vivo Characterization of 3D-Printed Polycaprolactone-Hydroxyapatite Scaffolds with Voronoi Design to Advance the Concept of Scaffold-Guided Bone Regeneration. *Frontiers in Bioengineering and Biotechnology* **2023**, *11*.

(19)   Ding, W.; Ge, Y.; Zhang, T.; Zhang, C.; Yin, X. Advanced Construction Strategies to Obtain Nanocomposite Hydrogels for Bone Repair and Regeneration. *NPG Asia Materials* **2024**, *16* (1), 14. https://doi.org/10.1038/s41427-024-00533-z.

(20)   Xu, H. H.; Wang, P.; Wang, L.; Bao, C.; Chen, Q.; Weir, M. D.; Chow, L. C.; Zhao, L.; Zhou, X.; Reynolds, M. A. Calcium Phosphate Cements for Bone Engineering and Their Biological Properties. *Bone Research* **2017**, *5* (1), 17056. https://doi.org/10.1038/boneres.2017.56.

(21)   Babilotte, J.; Martin, B.; Guduric, V.; Bareille, R.; Agniel, R.; Roques, S.; Héroguez, V.; Dussauze, M.; Gaudon, M.; Le Nihouannen, D.; Catros, S. Development and Characterization of a PLGA-HA Composite Material to Fabricate 3D-Printed Scaffolds for Bone Tissue Engineering. *Materials Science and Engineering: C* **2021**, *118*, 111334. https://doi.org/10.1016/j.msec.2020.111334.

(22)   Mazzoli, A. Selective Laser Sintering in Biomedical Engineering. *Medical & Biological Engineering & Computing* **2013**, *51* (3), 245–256. https://doi.org/10.1007/s11517-012-1001-x.

(23)   Laubach, M.; Hildebrand, F.; Suresh, S.; Wagels, M.; Kobbe, P.; Gilbert, F.; Kneser, U.; Holzapfel, B. M.; Hutmacher, D. W. The Concept of Scaffold-Guided Bone Regeneration for the Treatment of Long Bone Defects: Current Clinical Application and Future Perspective. *Journal of Functional Biomaterials* **2023**, *14* (7). https://doi.org/10.3390/jfb14070341.

(24)   Rezania, N.; Asadi-Eydivand, M.; Abolfathi, N.; Bonakdar, S.; Mehrjoo, M.; Solati-Hashjin, M. Three-Dimensional Printing of Polycaprolactone/Hydroxyapatite Bone Tissue Engineering Scaffolds Mechanical Properties and Biological Behavior. *Journal of Materials Science: Materials in Medicine* **2022**, *33* (3), 31. https://doi.org/10.1007/s10856-022-06653-8.

(25)   Joseph, B.; James, J.; Grohens, Y.; Kalarikkal, N.; Thomas, S. Additive Manufacturing of Poly (ε-Caprolactone) for Tissue Engineering. *JOM* **2020**, *72* (11), 4127–4138. https://doi.org/10.1007/s11837-020-04382-3.

(26)   Kim, M. H.; Yun, C.; Chalisserry, E. P.; Lee, Y. W.; Kang, H. W.; Park, S.-H.; Jung, W.-K.; Oh, J.; Nam, S. Y. Quantitative Analysis of the Role of Nanohydroxyapatite (nHA) on 3D-Printed PCL/nHA Composite Scaffolds. *Materials Letters* **2018**, *220*, 112–115. https://doi.org/10.1016/j.matlet.2018.03.025.

(27)   Agarwal, S.; Speyerer, C. Degradable Blends of Semi-Crystalline and Amorphous Branched Poly(Caprolactone): Effect of Microstructure on Blend Properties. *Polymer* **2010**, *51* (5), 1024–1032. https://doi.org/10.1016/j.polymer.2010.01.020.

(28)   Park, J. H.; Tucker, S. J.; Yoon, J.-K.; Kim, Y.; Hollister, S. J. 3D Printing Modality Effect: Distinct Printing Outcomes Dependent on Selective Laser Sintering (SLS) and Melt Extrusion. *Journal of Biomedical Materials Research Part A* **2024**, *112* (7), 1015–1024. https://doi.org/10.1002/jbm.a.37682.

(29)   Dias, J. R.; Sousa, A.; Augusto, A.; Bártolo, P. J.; Granja, P. L. Electrospun Polycaprolactone (PCL) Degradation: An In Vitro and In Vivo Study. *Polymers* **2022**, *14* (16). https://doi.org/10.3390/polym14163397.

(30)   Wang, F.; Tankus, E. B.; Santarella, F.; Rohr, N.; Sharma, N.; Märtin, S.; Michalscheck, M.; Maintz, M.; Cao, S.; Thieringer, F. M. Fabrication and

Characterization of PCL/HA Filament as a 3D Printing Material Using Thermal Extrusion Technology for Bone Tissue Engineering. *Polymers* **2022**, *14* (4). https://doi.org/10.3390/polym14040669.

(31) Gerdes, S.; Mostafavi, A.; Ramesh, S.; Memic, A.; Rivero, I. V.; Rao, P.; Tamayol, A. Process–Structure–Quality Relationships of Three-Dimensional Printed Poly(Caprolactone)-Hydroxyapatite Scaffolds. *Tissue Engineering Part A* **2020**, *26* (5–6), 279–291. https://doi.org/10.1089/ten.tea.2019.0237.

(32) Liu, D.; Nie, W.; Li, D.; Wang, W.; Zheng, L.; Zhang, J.; Zhang, J.; Peng, C.; Mo, X.; He, C. 3D Printed PCL/SrHA Scaffold for Enhanced Bone Regeneration. *Chemical Engineering Journal* **2019**, *362*, 269–279. https://doi.org/10.1016/j.cej.2019.01.015.

(33) Weng, L.; Teusink, M. J.; Shuler, F. D.; Parecki, V.; Xie, J. Highly Controlled Coating of Strontium-Doped Hydroxyapatite on Electrospun Poly(ε-Caprolactone) Fibers. *Journal of Biomedical Materials Research Part B: Applied Biomaterials* **2017**, *105* (4), 753–763. https://doi.org/10.1002/jbm.b.33598.

(34) Alshemary, A. Z.; Pazarceviren, A. E.; Tezcaner, A.; Evis, Z. Mesoporous Strontium Doped Nano Sized Sulphate Hydroxyapatite as a Novel Biomaterial for Bone Tissue Applications. *RSC Adv.* **2016**, *6* (72), 68058–68071. https://doi.org/10.1039/C6RA16809D.

(35) Bulina, N. V.; Khvostov, M. V.; Borodulina, I. A.; Makarova, S. V.; Zhukova, N. A.; Tolstikova, T. G. Substituted Hydroxyapatite and β-Tricalcium Phosphate as Osteogenesis Enhancers. *Ceramics International* **2024**. https://doi.org/10.1016/j.ceramint.2024.06.136.

(36) Zhou, X.; Wang, Z.; Li, T.; Liu, Z.; Sun, X.; Wang, W.; Chen, L.; He, C. Enhanced Tissue Infiltration and Bone Regeneration through Spatiotemporal Delivery of Bioactive Factors from Polyelectrolytes Modified Biomimetic Scaffold. *Materials Today Bio* **2023**, *20*, 100681. https://doi.org/10.1016/j.mtbio.2023.100681.

(37) Radulescu, D.-E.; Vasile, O. R.; Andronescu, E.; Ficai, A. Latest Research of Doped Hydroxyapatite for Bone Tissue Engineering. *International Journal of Molecular Sciences* **2023**, *24* (17). https://doi.org/10.3390/ijms241713157.

(38) Clark, R. A. F.; Ghosh, K.; Tonnesen, M. G. Tissue Engineering for Cutaneous Wounds. *Journal of Investigative Dermatology* **2007**, *127* (5), 1018–1029. https://doi.org/10.1038/sj.jid.5700715.

(39) Sell, S. A.; McClure, M. J.; Garg, K.; Wolfe, P. S.; Bowlin, G. L. Electrospinning of Collagen/Biopolymers for Regenerative Medicine and Cardiovascular Tissue Engineering. *Advanced Drug Delivery Reviews* **2009**, *61* (12), 1007–1019. https://doi.org/10.1016/j.addr.2009.07.012.

(40) Chartrain, N. A.; Williams, C. B.; Whittington, A. R. A Review on Fabricating Tissue Scaffolds Using Vat Photopolymerization. *Acta Biomaterialia* **2018**, *74*, 90–111. https://doi.org/10.1016/j.actbio.2018.05.010.

(41) Liu, T.; Jin, M.; Zhang, Y.; Weng, W.; Wang, T.; Yang, H.; Zhou, L. K+/Sr2+/Na+ Triple-Doped Hydroxyapatites/GelMA Composite Hydrogel Scaffold for the Repair of Bone Defects. *Ceramics International* **2021**, *47* (21), 30929–30937. https://doi.org/10.1016/j.ceramint.2021.07.277.

(42)   Chen, Q.; Zou, B.; Wang, X.; Zhou, X.; Yang, G.; Lai, Q.; Zhao, Y. SLA-3d Printed Building and Characteristics of GelMA/HAP Biomaterials with Gradient Porous Structure. *Journal of the Mechanical Behavior of Biomedical Materials* **2024**, *155*, 106553. https://doi.org/10.1016/j.jmbbm.2024.106553.

(43)   Zeugolis, D. I.; Paul, G. R.; Attenburrow, G. Cross-Linking of Extruded Collagen Fibers—A Biomimetic Three-Dimensional Scaffold for Tissue Engineering Applications. *Journal of Biomedical Materials Research Part A* **2009**, *89A* (4), 895–908. https://doi.org/10.1002/jbm.a.32031.

(44)   Allen, N. B.; Abar, B.; Johnson, L.; Burbano, J.; Danilkowicz, R. M.; Adams, S. B. 3D-Bioprinted GelMA-Gelatin-Hydroxyapatite Osteoblast-Laden Composite Hydrogels for Bone Tissue Engineering. *Bioprinting* **2022**, *26*, e00196. https://doi.org/10.1016/j.bprint.2022.e00196.

(45)   Uçak, N.; Çiçek, A.; Aslantas, K. Machinability of 3D Printed Metallic Materials Fabricated by Selective Laser Melting and Electron Beam Melting: A Review. *Journal of Manufacturing Processes* **2022**, *80*, 414–457. https://doi.org/10.1016/j.jmapro.2022.06.023.

(46)   Song, Y.; Ghafari, Y.; Asefnejad, A.; Toghraie, D. An Overview of Selective Laser Sintering 3D Printing Technology for Biomedical and Sports Device Applications: Processes, Materials, and Applications. *Optics & Laser Technology* **2024**, *171*, 110459. https://doi.org/10.1016/j.optlastec.2023.110459.

(47)   Mancuso, E.; Shah, L.; Jindal, S.; Serenelli, C.; Tsikriteas, Z. M.; Khanbareh, H.; Tirella, A. Additively Manufactured BaTiO3 Composite Scaffolds: A Novel Strategy for Load Bearing Bone Tissue Engineering Applications. *Materials Science and Engineering: C* **2021**, *126*, 112192. https://doi.org/10.1016/j.msec.2021.112192.

(48)   Rajan, K.; Samykano, M.; Kadirgama, K.; Harun, W. S. W.; Rahman, Md. M. Fused Deposition Modeling: Process, Materials, Parameters, Properties, and Applications. *The International Journal of Advanced Manufacturing Technology* **2022**, *120* (3), 1531–1570. https://doi.org/10.1007/s00170-022-08860-7.

(49)   Peltola, S. M.; Melchels, F. P. W.; Grijpma, D. W.; Kellomäki, M. A Review of Rapid Prototyping Techniques for Tissue Engineering Purposes. *Annals of Medicine* **2008**, *40* (4), 268–280. https://doi.org/10.1080/07853890701881788.

(50)   Fina, F.; Goyanes, A.; Gaisford, S.; Basit, A. W. Selective Laser Sintering (SLS) 3D Printing of Medicines. *International Journal of Pharmaceutics* **2017**, *529* (1), 285–293. https://doi.org/10.1016/j.ijpharm.2017.06.082.

(51)   Rane, K.; Strano, M. A Comprehensive Review of Extrusion-Based Additive Manufacturing Processes for Rapid Production of Metallic and Ceramic Parts. *Advances in Manufacturing* **2019**, *7* (2), 155–173. https://doi.org/10.1007/s40436-019-00253-6.

(52)   Whyman, S.; Arif, K. M.; Potgieter, J. Design and Development of an Extrusion System for 3D Printing Biopolymer Pellets. *The International Journal of Advanced Manufacturing Technology* **2018**, *96* (9), 3417–3428. https://doi.org/10.1007/s00170-018-1843-y.

(53)   Krishnanand; Singh, V.; Mittal, V.; Branwal, A. K.; Taufik, M. Extruder Design in Pellets Operated 3D Printers: A Review. In *Proceedings of the International Conference on Industrial and Manufacturing Systems (CIMS-2020)*; Pratap Singh, R., Tyagi, D. M.,

Panchal, D., Davim, J. P., Eds.; Springer International Publishing: Cham, 2022; pp 661–675.

(54)   Chen, H.; Guo, L.; Zhu, W.; Li, C. Recent Advances in Multi-Material 3D Printing of Functional Ceramic Devices. *Polymers* **2022**, *14* (21). https://doi.org/10.3390/polym14214635.

(55)   Singamneni, S.; Behera, M. P.; Truong, D.; Le Guen, M. J.; Macrae, E.; Pickering, K. Direct Extrusion 3D Printing for a Softer PLA-Based Bio-Polymer Composite in Pellet Form. *Journal of Materials Research and Technology* **2021**, *15*, 936–949. https://doi.org/10.1016/j.jmrt.2021.08.044.

(56)   Liaw, C.-Y.; Guvendiren, M. Current and Emerging Applications of 3D Printing in Medicine. *Biofabrication* **2017**, *9* (2), 024102. https://doi.org/10.1088/1758-5090/aa7279.

(57)   Goodarzi Hosseinabadi, H.; Nieto, D.; Yousefinejad, A.; Fattel, H.; Ionov, L.; Miri, A. K. Ink Material Selection and Optical Design Considerations in DLP 3D Printing. *Applied Materials Today* **2023**, *30*, 101721. https://doi.org/10.1016/j.apmt.2022.101721.

(58)   Levato, R.; Dudaryeva, O.; Garciamendez-Mijares, C. E.; Kirkpatrick, B. E.; Rizzo, R.; Schimelman, J.; Anseth, K. S.; Chen, S.; Zenobi-Wong, M.; Zhang, Y. S. Light-Based Vat-Polymerization Bioprinting. *Nature Reviews Methods Primers* **2023**, *3* (1), 47. https://doi.org/10.1038/s43586-023-00231-0.

(59)   Gu, Z.; Fu, J.; Lin, H.; He, Y. Development of 3D Bioprinting: From Printing Methods to Biomedical Applications. *Asian Journal of Pharmaceutical Sciences* **2020**, *15* (5), 529–557. https://doi.org/10.1016/j.ajps.2019.11.003.

(60)   Zhang, Y.; Li, M.; Tseng, T.-M.; Schlichtmann, U. Open-Source Interactive Design Platform for 3D-Printed Microfluidic Devices. *Communications Engineering* **2024**, *3* (1), 71. https://doi.org/10.1038/s44172-024-00217-0.

(61)   Haudum, S.; Demirdögen, B.; Müller-Müchler, L.; Döttl, S. C.; Müller, S. M.; Naderer, C.; Brüggemann, O.; Griesser, T.; Jacak, J.; Priglinger, E.; Teasdale, I. Biodegradable Resins for Photochemical 3D Printing via Vinyl Ester and Vinyl Carbonate Functionalized Amino Acid-Phosphoramidates. *European Polymer Journal* **2024**, *211*, 113037. https://doi.org/10.1016/j.eurpolymj.2024.113037.